SEARCHING FOR TOP SQUARKS AT THE LARGE HADRON COLLIDER

A Dissertation

by

KECHEN WANG

Submitted to the Office of Graduate and Professional Studies of
Texas A&M University
in partial fulfillment of the requirements for the degree of

DOCTOR OF PHILOSOPHY

Chair of Committee,	Bhaskar Dutta
Committee Members,	Teruki Kamon
	Dimitri Nanopoulos
	Stephen Fulling
Head of Department,	George Welch

August 2014

Major Subject: Physics

ABSTRACT

This dissertation describes the search strategies we developed for the lighter top squark (called stop, or $\tilde{t}$) at the Large Hadron Collider (LHC). When the lighter top squarks are produced from the cascade decay of gluino and squark, the analysis is performed in the stop-neutralino coannihilation region where stop decays into a charm quark and the stable lightest supersymmetric particle (called lightest neutralino, or $\tilde{\chi}_1^0$). We develop observables through the endpoint measurements to determine the stop masses.

When the lighter top squarks are produced from the direct production processes of stop pairs ($\tilde{t}\tilde{t}^*$), three scenarios are investigated. In the fully hadronic final state scenario, we investigate the identification of stops which decay predominantly into a top quark and the stable lightest neutralino. A simple kinematical variable, M3, is used to reconstruct two top quarks which are pair-produced from the stops in the fully hadronic channel. We identify kinematical variables to reduce the standard model (SM) background. The expected mass reach of stop is shown at 8-TeV LHC (LHC8).

In the Bino-Higgsino dark matter scenario, the lightest neutralino is a mixture of Bino and Higgsino, satisfying the thermal dark matter relic density. Stop can decay into a top quark plus the second or third lightest neutralino (called $\tilde{\chi}_2^0$, $\tilde{\chi}_3^0$), and the second or third lightest neutralino can decay into 2 leptons plus the lightest neutralino via an intermediate slepton ("light selpton" case) or Z boson ("heavy slepton" case). The final states have at least 2 jets, 2 opposite-sign same flavor leptons and missing energy. The opposite-sign same flavor dilepton mass distribution after subtracting the opposite-sign different flavor distribution shows a clear edge in the case of light slepton. We also calculate the significance at LHC8 for discovering such a scenario in both light slepton case and heavy slepton case.

In the compressed scenario where the mass difference between stop and the lightest neutralino is approximately equal to the mass of the top quark, stop does either the two-body decay of a top quark, and the lightest neutralino ("two-body decay" case, when mass difference is slightly greater than the top quark mass), or the three-body decay of a bottom quark, a W boson and

the lightest neutralino ("three-body decay" case, when the mass difference is smaller than the top quark mass). We perform the study for both two-body and three-body decay cases in the final state of two b-jets, one lepton, large missing energy, and two high energetic Vector Boson Fusion tagging jets with large separation in pseudo-rapidity, in opposite hemispheres, and with large dijet mass. The expected experiment discovery and exclusion limits of such a compressed scenario are shown at 14-TeV LHC (LHC14) for both cases.

DEDICATION

To my parents for their love and for providing me the environment to pursue my own interests,

To my elder sister for her love and for taking care of my parents when I was so far,

To Bhaskar for his guidance and for crating a healthy climate for productive work,

To my friends for their care and encouragement.

ACKNOWLEDGEMENTS

I would like to acknowledge the guidance and support of my dissertation advisor Bhaskar Dutta. I am also grateful to the rest of my committee: Teruki Kamon, Dimitri Nanopoulos and Stephen Fulling. I do appreciate the help of Richard Arnowitt.

At the beginning of my graduate study, I received lots of assistance from Abram Krislock. Kuver Sinha also helped me a lot. I want to thank them.

I also want to thank Sean Downes and Sheldon Campbell for sharing their document formatting files such that my thesis can meet the thesis office guidelines.

Finally, a big thank you to all my friends who cared about me and encouraged me during my graduate study.

TABLE OF CONTENTS

Page

LIST OF FIGURES

Page

LIST OF TABLES

CHAPTER I

INTRODUCTION

The LHC is testing many ideas for physics beyond the standard model (SM). Of these, low energy Supersymmetry (SUSY) is the best motivated candidate for new TeV scale physics, as it addresses the hierarchy problem, gives gauge coupling unification, and (in R-parity conserving models) provides a robust dark matter candidate.

The LHC has also observed a new boson consistent with the SM Higgs, with mass in the region of 125 GeV [1]. In the SM, higher loop corrections to the Higgs mass are quadratically divergent. The problem is most severe in the case of the one-loop correction from the third generation top sector, since other contributions to the Higgs mass are suppressed by gauge or smaller Yukawa couplings. To avoid fine-tuning, new physics should appear around a scale of $\mathcal{O}(1)$ TeV and cut off the divergences. The most widely studied mechanism for cancelling the divergences is SUSY, and in particular the dangerous top quark loops are cancelled by the scalar superpartner of the top quark, called top squark. Thus, reducing fine-tuning in the SM leads minimally to the conclusion that there should be a partner for the top quark around the TeV regime which is responsible for the cancellations.

Given its importance in stabilizing the Higgs mass, probing the lighter superpartner of top quark is a high-priority study at the LHC. Results from the 8-TeV LHC (LHC8) have put bounds on the masses of the colored superpartners. The exclusion limits on squark and gulino masses, when they are comparable, are approximately 1.5 TeV at 95% CL with 20 fb^{-1} of integrated luminosity [2, 3, 4, 5]. On the other hand, due to the small production cross section of stop pairs and a huge background from top quark production, the exclusion bounds on the mass of the lighter top squark are much more modest [6, 7]. The projected top squark discovery mass reach and exclusion plots for the high-luminosity LHC have been studied by the ATLAS [8] and CMS [9] Collaborations.

Throughout this dissertation, we will always be speaking about the lighter top squark ($\tilde{t}_1$), which we will hereafter call $\tilde{t}$. We have developed a number of analysis strategies for the lighter top squark in the last few years. The rest of this dissertation will describe these strategies in details. Based on our work in [10], in Chapter II, we investigate the $\tilde{t}$ search from the cascade decay of gluino and squark in the stop-neutralino coannihilation scenario. The $\tilde{t}$ produced from the direct production processes of stop pairs ($\tilde{t}\tilde{t}^*$) is investigated in the following chapters. In Chapter III, we describe the $\tilde{t}$ search in the fully hadronic final state scenario. This chapter is based on our work in [11]. The search strategy of $\tilde{t}$ in Bino-Higgsino dark matter scenario is presented in Chapter IV, which is firstly reported in our work [12]. In Chapter V, we will show a feasibility study in the compressed scenario where the mass difference between $\tilde{t}$ and $\tilde{\chi}_1^0$ is approximately equal to mass of top quark. This is firstly discussed in our work [13]. The summary and conclusion are in Chapter VI.

CHAPTER II

TOP SQUARK SEARCH FROM CASCADE DECAY*

In this chapter, we determine stop mass through endpoint measurements of kinematic observables arising from cascade decay. The analysis is performed in the stop-neutralino coannihilation scenario where the mass difference between stop and lightest neutralino is very small, $m_{\tilde{t}} - m_{\tilde{\chi}_1^0} < m_W$. Lightest neutralino is considered to be mostly Bino and next lightest neutralino is mostly Wino, the Higgsino components are negligible. The dark matter relic density is satisfied by the coannihilation mechanism. In this region, stop decays into a charm quark and the lightest neutralino. we thus develop observables to determine stop masses. This analysis is based on our work in [10].

II.1 Benchmark Points in Stop-neutralino Coannihilation Scenario

The measurement of third generation squark masses presents its own challenges. Reconstruction of stop ($\tilde{t}$) and sbottom ($\tilde{b}$) is very hard in a cascade decay chain since both stops and sbottoms decay into b quarks. Moreover, to make the situation worse, in the stop-neutralino coannihilation scenario the stop decay produces a lower p_T jet due to the proximity of the stop and the lightest neutralino masses. We invoke two new observables to measure stop and sbottom masses in the cascade decays.

We choose points that satisfy the stop-neutralino coannihilation constraints. We use DarkSUSY [14] to select exact benchmark points in the above region which give the correct dark matter relic density. The mass spectrum at the stop coannihilation benchmark point is shown in Table II.1.

Since $\tan\beta$ is on the large side for the benchmark points, the lighter stau mass is between the lightest and next to lightest neutralinos. The mass spectrum of the model is determined using ISAJET [15]. The spectrum is then fed to PYTHIA [16], which generates the Monte Carlo hard

*Parts of this chapter are reprinted with permission from "*Diagnosis of Supersymmetry Breaking Mediation Schemes by Mass Reconstruction at the LHC*", by B. Dutta, T. Kamon, A. Krislock, K. Sinha and K. Wang, Phys. Rev. D **85**, 115007 (2012), Copyright 2012 by The American Physical Society.

Table II.1: Spectrum at a stop coannihilation benchmark point. All masses are in GeV.

Particle	Mass	Particle	Mass	Particle	Mass
$\tilde{d}_L$	653	$\tilde{e}_L$	437	$\tilde{\chi}_1^0$	286
$\tilde{d}_R$	636	$\tilde{e}_R$	411	$\tilde{\chi}_2^0$	338
$\tilde{u}_L$	648	$\tilde{\tau}_1$	315	$\tilde{\chi}_3^0$	477
$\tilde{u}_R$	635	$\tilde{\tau}_2$	418	$\tilde{\chi}_4^0$	503
$\tilde{b}_1$	520			$\tilde{\chi}_1^\pm$	337
$\tilde{b}_2$	596			$\tilde{\chi}_2^\pm$	500
$\tilde{t}_1$	339			$\tilde{g}$	650
$\tilde{t}_2$	616				

scattering events and hadron cascade. These events are passed to the detector simulator PGS4 [17].

Note that our methods are valid in general, and the above benchmark points will be explored as an illustration. In particular, we will also a study benchmark point with higher mass spectrum, preferred by current LHC data in Subsection II.3.3, where we will show that we need larger luminosity to establish the same set of observables.

II.2 Search Strategy

In this section, we present the measurement of physical observables which will be used to solve for the $\tilde{t}$ masses. We will also give results for a benchmark point with heavier mass spectrum.

II.2.1 Event Selection

To probe the third generation squark masses we need to involve b quarks. The relevant decay chain associated with the dominant production process for the reconstruction of third generation squarks in the stop coannihilation region is

$$\tilde{g} \to \tilde{b} + b \to \tilde{t} + W + b \to \tilde{\chi}_1^0 + c + W + b \tag{II.1}$$

These signals are characterized by high p_T jets accompanied by a W and $\not{E}_T$. We will be considering the full supersymmetric contribution and using Bi-Event Subtraction Technique (BEST) [18] to identify and reconstruct a W. We will then be constructing the distributions M_{bW} and M_{jW}. The cuts for the analysis are

(i) $\not{E}_T \geq 180$ GeV;

(ii) Number of jets: $N_{jets} \geq 4$;

(iii) Leading jet cuts: the first two leading jets each have $p_T \geq 200$ GeV in $|\eta| \leq 2.5$. They could be gluon, light-flavour, or b jets;

(iv) Soft jet cuts: Any jets with $p_T \geq 30$ GeV in $|\eta| \leq 2.5$ are accepted in the analysis. This includes b-tagged jets;

(v) $p_{T,jet1} + p_{T,jet2} + \not{E}_T \geq 600$ GeV;

(vi) For M_{bW}, at least one tight b-tagged jet is required.

We next reconstruct the mass of $j + W$ (and $b + W$) system in the sample of events that pass the above selection cuts. As shown in [18, 19], the use of BEST twice to reconstruct the $j + W$ (or $b + W$) system is found to be very powerful in handling combinatorial background to extract the endpoint in the M_{jW} distribution and top mass peak in the M_{bW} distribution.

The first step in the analysis is the reconstruction of the W boson. The W appears in the detector as two jets whose invariant mass falls in the W mass window (65 GeV $\leq M_{jj} \leq$ 90 GeV). We thus choose soft jet pairs (from the third leading jet and below) which are not b-tagged, with $0.4 \leq \Delta R \leq 1.5$. The jets are put into two categories: whose which are manifestly in the W window, and those that fall within the sideband window (40 GeV $\leq M_{jj} \leq$ 55 GeV or 100 GeV $\leq M_{jj} \leq$ 115 GeV). BEST is then performed for the two categories, to git rid of uncorrelated jet background. After this, the sideband subtraction is performed to obtain the W mass.

Once the W is reconstructed, it is paired up with jets to form the M_{bW} and M_{jW} distributions.

II.2.2 M_{jW} *Distribution*

For the M_{jW} distribution, we pair the W with a non b-tagged soft jet, whose rank is three or lower. This is because we are in the stop coannihilation region. In Figure II.1, we show the M_{jW} distribution at the benchmark point, finding a well defined endpoint for 50 fb^{-1} luminosity.

Figure II.1: Distribtuion of M_{jW} at a stop coannihilation benmark point. W is firstly reconstructed with two jets whose invariant mass falls in the W window. The reconstructed W is then combined with a non b-tagged soft jet of rank three or lower from the same event, to produce the same-event blue histogram. The W is combined with a soft jet from a different event to produce the bi-event filled dot-dashed blue (grey) histogram, which is normalised to the shape of the long tail of the same-event histogram. The same-event minus bi-event subtraction produces the black subtracted histogram. The subtracted histogram is fitted with a straight line to obtain the endpoint. The result from the endpoint is 287.55 ± 0.74 (Stat.) GeV. The luminosity is 50 fb^{-1}.

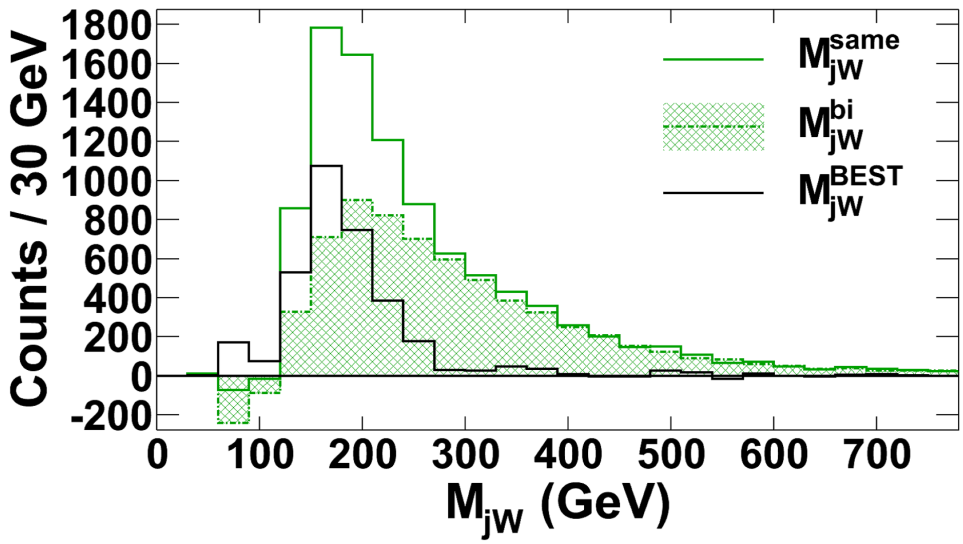

II.2.3 M_{bW} Distribution

For the M_{bW} distribution, we pair the W with a b jet of any rank form the current event. Note that the relevant b jet required to construct this observable need not be a leading jet; in fact, the leading jet will typically be non b-tagged. After pairing the W with the b jet, we do a further BEST to get rid of uncorrelated b jets. This gives the final signal for M_{bW}. However, the b+W signal shows the presence of the unwanted top peak, which comes form $t \to b + W$. The top window is removed from the final signal, by discarding events with $M_{bW} \leq 200$ GeV. In Figure II.2, we show the M_{bW} distribution obtained at the benchmark point, finding the endpoint for 50 fb^{-1} luminosity.

Figure II.2: Distribtuion of M_{bW} at a stop coannihilation benmark point. W is firstly reconstructed with two jets whose invariant mass falls in the W window. The reconstructed W is then combined with a b jet of any rank from the current event, to produce the same-event pink histogram. Events with $M_{bW} \leq 200$ GeV are discarded to remove the top peak. The W is combined with a b jet from a different event to produce the bi-event filled dot-dashed pink (grey) histogram, which is normalised to the shape of the long tail of the same-event histogram. The same-event minus bi-event subtraction produces the black subtracted histogram. The subtracted histogram is fitted with a straight line to obtain the endpoint. The result from the endpoint is 325.67 ± 4.50 (Stat.) GeV. The luminosity is 50 fb^{-1}.

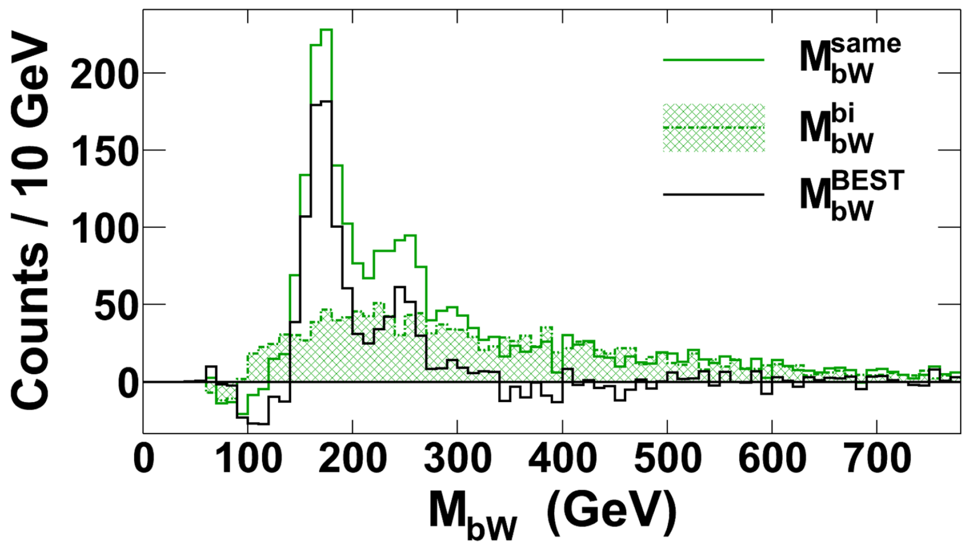

II.3 Results

II.3.1 Kinematical Observables

In Table II.2, we show the endpoint values obtained from these distributions. The statistical uncertainties range between $0.2\% - 1.4\%$. The statistical uncertainty is larger for M_{bW} due to the b jet.

II.3.2 Determination of $\tilde{t}$ Masses

The observables M_{bW}^{end} and M_{jW}^{end} are used to determine the third generation squark masses, once the gaugino (i.e., gluino and lightest neutralino) masses have been obtained with other observables. Theoretically, the functional dependences are $M_{bW} = M_{bW}(m_{\tilde{b}}, m_{\tilde{t}}, m_{\tilde{g}})$ and

Table II.2: Kinematical observables M_{jW}^{end} and M_{bW}^{end} at 50 fb^{-1} for a stop coannihilation benchmark point. All masses are in GeV.

Observable	Value	50 fb^{-1} Stat.	100 fb^{-1} Stat.
M_{jW}^{end}	287.55	0.74	0.52
M_{bW}^{end}	325.67	4.50	3.18

$M_{jW} = M_{jW}(m_{\tilde{b}}, m_{\tilde{t}}, m_{\tilde{\chi}_1^0})$. The stop and sbottom masses are varied independently around the benchmark point, and the collider experiment is simulated and determination of M_{bW}^{end} and M_{jW}^{end} is performed each time to get the functional relations between the kinematical observables and masses. We then find the solutions of stop and sbottom masses using Nelder-Mead method from these functions. We show the masses of third generation squarks with uncertainties in Table II.3. The statistical uncertainties range between $2.5\% - 11.3\%$.

Table II.3: Solution to stop and sbottom masses at 50 fb^{-1} for a stop coannihilation benchmark point. All masses are in GeV.

Particle	Mass	50 fb^{-1} Stat.	100 fb^{-1} Stat.
$\tilde{b}$	531	-60, +60	-47, +47
$\tilde{t}$	326	-5, +8	-4, +7

II.3.3 *Results for A Heavy Mass Spectrum*

Upto this point, we have displayed our techniques of reconstructing masses at the benchmark point given in Table II.1. Our techniques work perfectly well at benchmark points with higher mass spectrum, as preferred by current LHC data. Higher luminosity is of course required to obtain endpoints. Below, in Table II.4, we choose such a benchmark point with $m_{\tilde{g}} \sim 1.2$ TeV, and show solutions of the masses of third generation squarks.

For this benchmark point in Table II.4, a luminosity of 200 fb^{-1} is required to solve for all the masses, following the techniques we have shown in this chapter. We show the masses we obtained for this benchmark point in Table II.5. The statistical uncertainties range between $0.9\% - 14.7\%$.

Table II.4: Model parameters and spectrum at a new stop coannihilation benchmark point with heavier gluino. All masses are in GeV.

Particle	Mass	Particle	Mass	Particle	Mass
$\tilde{d}_L$	1190	$\tilde{e}_L$	888	$\tilde{\chi}_1^0$	666
$\tilde{d}_R$	1169	$\tilde{e}_R$	850	$\tilde{\chi}_2^0$	740
$\tilde{u}_L$	1188	$\tilde{\tau}_1$	721	$\tilde{\chi}_3^0$	836
$\tilde{u}_R$	1167	$\tilde{\tau}_2$	840	$\tilde{\chi}_4^0$	870
$\tilde{b}_1$	980			$\tilde{\chi}_1^\pm$	739
$\tilde{b}_2$	1084			$\tilde{\chi}_2^\pm$	868
$\tilde{t}_1$	705			$\tilde{g}$	1187
$\tilde{t}_2$	1044				

Table II.5: Solution to stop and sbottom masses at 200 fb^{-1} for a stop coannihilation benchmark point with heavier gluino. All masses are in GeV.

Particle	Mass	200 fb^{-1} Stat.
$\tilde{b}$	690	± 6
$\tilde{t}$	1002	± 126

CHAPTER III

FULLY HADRONIC FINAL STATE SCENARIO*

At the LHC, it is expected that the existence of stops will be indirectly established initially using inclusive jets + single lepton + $\not{E}_T$ analysis. However, once any excess is observed, the direct evidence of the stop can be established through the existence of top quarks in the signal. Our goal in this chapter is to establish the existence of two top quarks in the final states along with the missing energy in all hadronic channel.

We will probe a technique for stop searches in the following decay mode

$$\tilde{t} \to t + \tilde{\chi}_1^0, \tag{III.1}$$

where the $\tilde{\chi}_1^0$ is the lightest neutralino, which we will take to be the lightest supersymmetric particle (LSP). In R-parity conserving models, the LSP is the main source of missing energy in the event. We will not make any assumptions about the spectrum, except that the above decay mode is kinematically allowed and dominant.

In this chapter, top squark searches will be carried out in the scenario where the $\tilde{\chi}_1^0$ is mainly a Bino and the second lightest neutralino ($\tilde{\chi}_2^0$) mainly a Wino. In such a scenario, the top squark $\tilde{t}$ decays to $\tilde{\chi}_1^0$ and a top (t) quark at a branching fraction ($\mathcal{B}$) of nearly 100%.

The main challenge in such searches is the fact that the LHC is a top quark factory and distinguishing top quarks produced from stop decay, as opposed top quarks produced directly, can be very difficult. There are several established techniques of probing the $t\bar{t}$ system or identifying top quarks. We use the trijet invariant mass M3 to explicitly reconstruct the two-top quark system from the stops decay in fully hadronic final state of events with at least four non-b jets, at least two b jets, and large missing energy.

*Parts of this chapter are reprinted with permission from "*Searching for Top Squarks at the LHC in Fully Hadronic Final State*", by B. Dutta, T. Kamon, N. Kolev, K. Sinha and K. Wang, Phys. Rev. D **86**, 075004 (2012), Copyright 2012 by The American Physical Society.

Our finding is that simple kinematical selections with the M3 variable is an effective tool for stop searches. At $\sqrt{s} = 8$ TeV, we achieve background and signal cross-sections at comparable levels for stop masses around $350 - 500$ GeV. These results was originally reported in our work [11].

M3 is defined as the invariant mass of trijet combinations with highest vectorically summed p_T. M3 has been used in top quark studies at CMS [20] and CDF [21]. For the two quark system in Equation III.1, the highest p_T jets are most likely to be from the top quark, if it is signal. Intuitively, M3 should work well in such a system.

III.1 Benchmark Points and Background

The benchmark points we will use are listed in Table III.1. Signal events are generated with ISAJET + PYTHIA.

Table III.1: Benchmark points for study in fully hadronic final state. All masses are in GeV.

$\tilde{t}$	350	400	450	500	550	400	400
$\tilde{\chi}_1^0$	100	100	100	100	100	150	200

We generate the following SM backgrounds with ALPGEN [22] + PYTHIA: W + n jets, Z + n jets and $t\bar{t}$ + n jets, with $n \leq 6$, as well as single top + jets. The background cross sections are listed in Table III.2. Interestingly, we noticed that after all cuts $t\bar{t} + (3-6)$ jets contribution to the background is comparable to $t\bar{t} + (0-2)$ jets.

Table III.2: Main sources of background. "Others" includes single top + jets, W + n jets and Z + n jets with $1 \leq n \leq 6$. All cross sections are in fb.

Background	$t\bar{t} + (\leq 2)j$	$t\bar{t} + (3-6)j$	Others
Cross section	2.0×10^5	0.24×10^5	2.8×10^6

In order to make our analysis realistic we use PGS4 detector simulation both for the signal and background events.

III.2 Search Strategy

We consider the fully hadronic mode

$$pp \to \tilde{t}\tilde{t}^* \to (t\tilde{\chi}_1^0)(\bar{t}\tilde{\chi}_1^0) \to (bjj\tilde{\chi}_1^0)(\bar{b}jj\tilde{\chi}_1^0), \tag{III.2}$$

We firstly select the events with at least four non-b jets, at least two b-tagged jets, and large missing energy $\not{E}_T$.

The main source of missing energy for the $t\bar{t}$ background are neutrinos coming from the leptonic decay of W bosons, while for the signal the dominant source of missing energy is the neutralino. Clearly, after the missing energy cut, the most critical factor affecting the discrimination of signal over background in the fully hadronic mode is the lepton veto efficiency. Due to imperfections of the lepton veto, $t\bar{t}$ events with leptonic W decay could be a dominant source of background.

Our method is to (1) reconstruct a top quark using the trijet invariant mass M3, (2) use kinematic correlations between the constituents of the two (bjj) systems and $\not{E}_T$ to improve the reconstruction of the pair of top quarks and (3) finally apply M3 again to identify the second top quark. We describe these steps below, before showing our results in the next section.

(1) We use M3 twice. First, combinations of three jets are made in the sample, keeping one b-tagged jet and two untagged jets in each trijet combination. Next, the trijet combination with the largest vectorically summed transverse momentum $p_{T,bjj}^{leading}$ is chosen. The invariant mass of this trijet combination is defined as $M3(p_{T,bjj}^{leading})$. It approximates the mass of the hadronically decaying top quark. Similarly, we find a 2nd leading trijet combination $p_{T,bjj}^{2nd}$. Associated with M3, we also define M2, which is the invariant mass of the two untagged jets in the trijet M3 combination.

Using M3, we identify a first top quark, which we call "System A". This is done by calculating χ^2 for the trijet and dijet combination corresponding to the leading p_T combination $M3(p_{T,bjj}^{leading})$ and also for the 2nd leading combination $M3(p_{T,bjj}^{2nd})$, with a mean top quark mass of 170 GeV and width of 15 GeV, and a mean W mass of 80 GeV and a width of 10 GeV. the combination with the lowest χ^2 is then taken to represent System A. We call this combination $M3^{min}$.

Figure III.1: [Left] schematic diagram of the signal. The stop pair gives rise to $t\bar{t}$ and neutralinos, which are the main source of $\not{E}_T$. In the fully hadronic mode, the top quarks decay into trijet systems. "System A" is the trijet system containing the leading p_T jet and reconstructed using M3, while the remaining jets are called "System B". [Right] $t\bar{t}$ background after lepton veto where the lepton is undetected. The main source of $\not{E}_T$ here is the neutrino from W decaying leptonically. The associated lepton passing the veto is termed a "lost lepton".

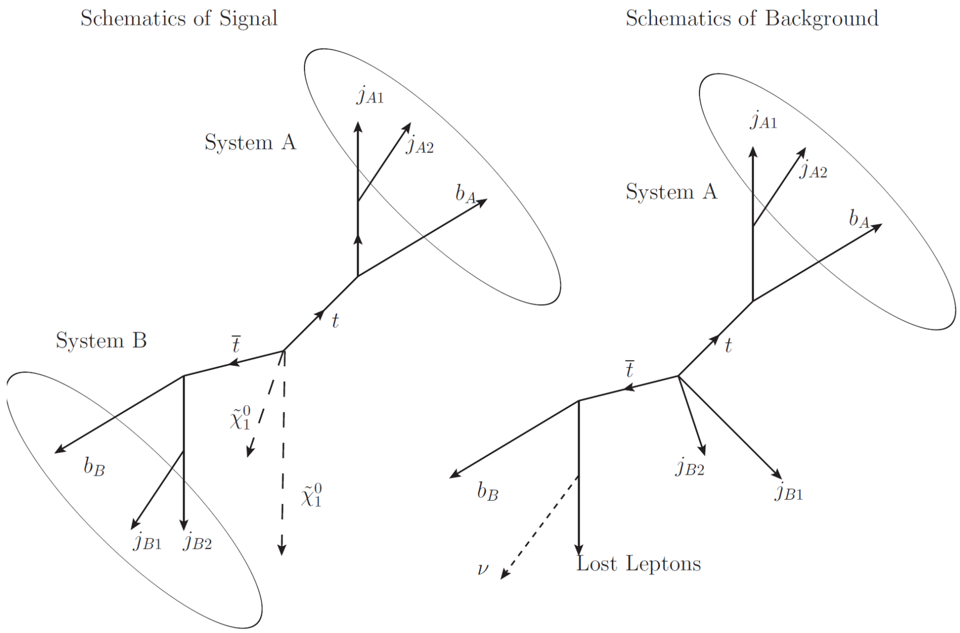

We note that this χ^2 analysis allows for more signal events in the identification of System A. We show the results of this analysis in Section III.3.

(2) After the identification of System A, we classify the remaining b-jet and non b-tagged jets to be "System B"; thus, we would denote them as $(b_B j_B j_B)$. We employ various cuts on azimuthal angles between jets and $\not{E}_T$, and M_T between b_B and $\not{E}_T$. These are motivated by the fact that for signal, the main source of missing energy is the neutralino, while for the $t\bar{t}$ background, the main source of missing energy is the neutrino coming form the leptonic decay of the W, or from jet mismeasurement. Thus, for example, for the background, $\not{E}_T$ is aligned along b_B, as is clear from the schematic diagram shown in Figure III.1. For the stop decay, however, the correlation between the $\not{E}_T$ in the form of neutralino and the b_B is far weaker. The results of this analysis are shown in Section III.3.

(3) At the final stage, we apply M3 again to identify the second top quark, System B. The result

of this analysis is shown in Section III.3.

III.3 Results

In this section, we describe our selection criteria and the cross sections after every stage of cuts (see Table III.5).

III.3.1 Baseline Cuts: 6 Jets, Lepton Veto, $\not{E}_T$

Our baseline selection cuts are:

(i) $N_{nonb-jets} \geq 4$, and at least two loosely tagged b-jets.

(ii) The leading jet has $p_T > 100$ GeV in $|\eta| \leq 2.5$, and all other jets have $p_T > 30$ GeV in $|\eta| \leq 2.5$.

(iii) Lepton veto: We reject isolated electrons and muons with $p_T > 10$ GeV in $|\eta| \leq 2.5$. The isolation criteria are $\Sigma p_{T,iso}^{track} \leq 5$ GeV with $\Delta R = 0.4$.

(iv) τ veto: We also reject any hadronically decaying τ with $p_T > 20$ GeV in $|\eta| \leq 2.1$. We assume a identification efficiency of 60% and a fake rate of 2%.

(v) $\not{E}_T \geq 100$ GeV.

III.3.2 M3: Tagging Top System A

In this section, we use M3 to tag the top quark in System A, after a $\not{E}_T$ cut to further reduce SM background. The value of the $\not{E}_T$ cut is determined by maximizing the significance for each choice of mass. This is shown in Table III.3.

Table III.3: $\not{E}_T$ cuts for various choices of masses. All masses are in GeV.

$\tilde{t}$	350	400	450	500	550	400	400
$\tilde{\chi}_1^0$	100	100	100	100	100	150	200
$\not{E}_T$ cut	145	170	195	195	195	170	100

As described in Section III.2, we identify System A by using M3. Figure III.2 shows the comparative distributions of $M3^{min}$ and $M3(p_{T,bjj}^{leading})$. We improve the top tagging by approximately 30% in signal events in the top quark mass region.

Figure III.2: Distributions of $M3^{min}$ and $M3(p_{T,bjj}^{leading})$. The inset shows the distribution after M2 mass window cut. A gain of ~ 30% in signal is obtained by using $M3^{min}$. The luminosity is 50 fb^{-1}.

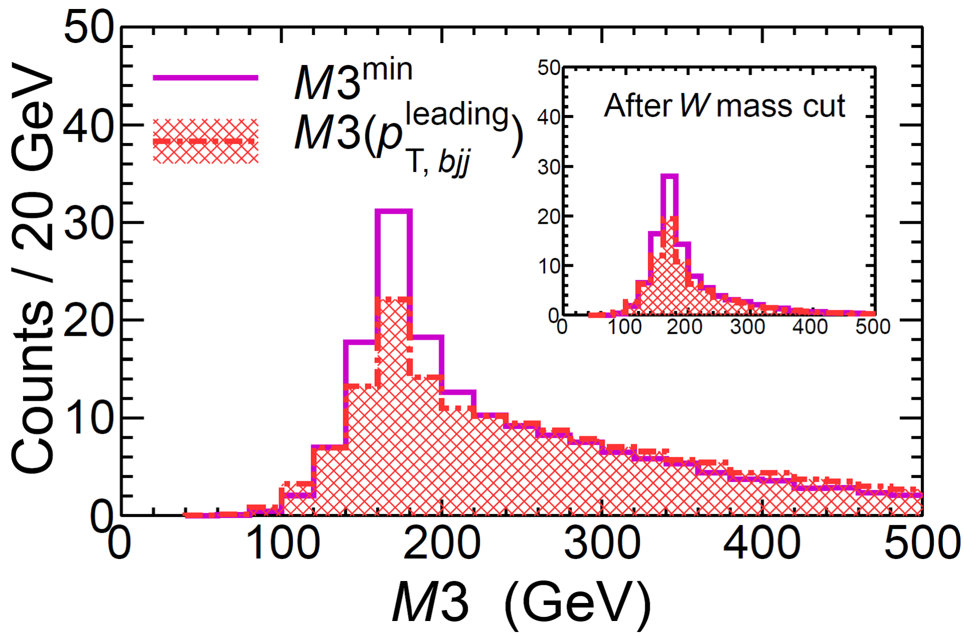

We next perform a W mass window cut on $M2^{min}$, taking 40 GeV $\le M2^{min} \le$ 120 GeV and a top quark mass window cut on $M3^{min}$, taking 120 GeV $\le M3^{min} \le$ 220 GeV. We show the $M3^{min}$ distribution after $M2^{min}$ mass cut in the inset of Figure III.2. We now proceed to probe the constituents of the "other top quark" in System B.

III.3.3 Angular and M_T Cuts: Kinematic Correlations between $\not{E}_T$ and Jets

We denote the remaining b-jet and non b-tagged jets as $(b_B j_B j_B)$. We clean up the system with various angular and M_T cuts, as mentioned in our search strategy in Section III.2. The cuts values are chosen based on Figure III.3 and III.4:

(i) $\Delta\phi(b_B, \not{E}_T) > 1.2$ and $\Delta\phi(j_{B(1,2)}, \not{E}_T) > 0.7$, where $j_{B(1,2)}$ refer to the first and second leading jets in System B, respectively.

(ii) $M_T(b_B, \not{E}_T)$: We choose optimal cut values for different masses (see Table III.4).

Figure III.3: Distributions of $\Delta\phi(b_B, \not{E}_T)$, $\Delta\phi(j_{B1}, \not{E}_T)$, and $\Delta\phi(j_{B2}, \not{E}_T)$ for $t\bar{t}$ background and signal ($m_{\tilde{t}} = 400$ GeV, $m_{\tilde{\chi}_1^0} = 100$ GeV). We cut at $\Delta\phi(b_B, \not{E}_T) > 1.2$, $\Delta\phi(j_{B(1,2)}, \not{E}_T) > 0.7$. Here, b_B, j_{B1} and j_{B2} denote the b, leading jet, and next leading jet of System B. The luminosity is 50 fb^{-1}.

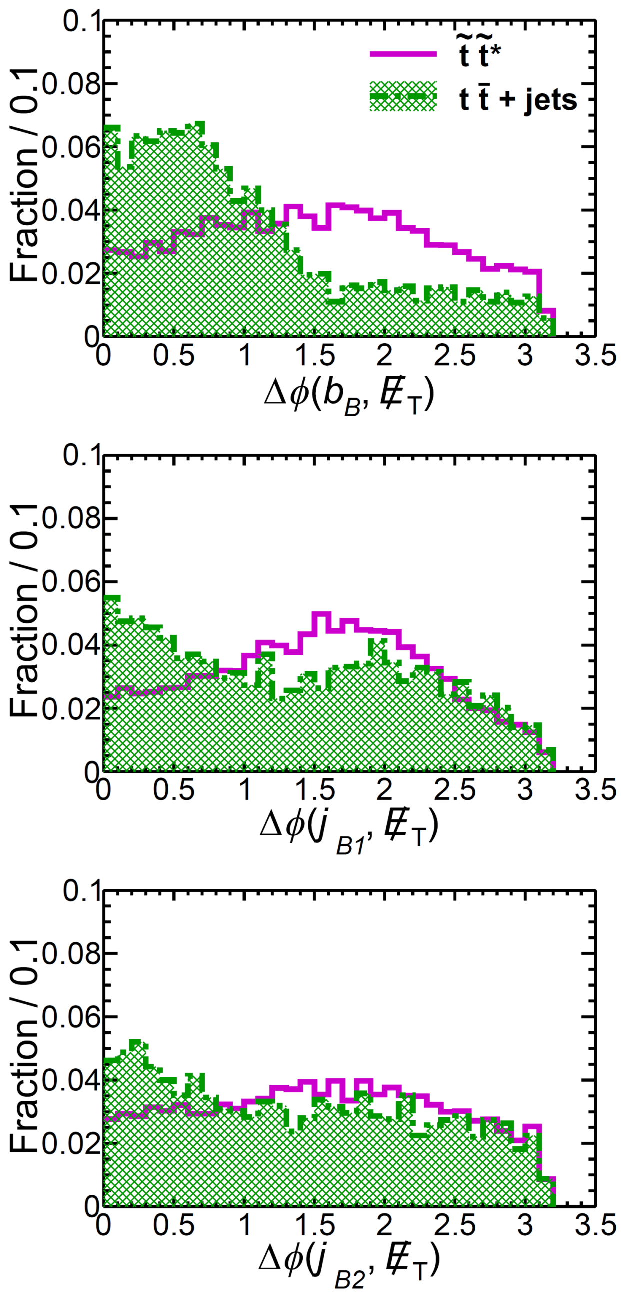

Figure III.4: Distributions of $M_T(b_B, \not{E}_T)$ for $t\bar{t}$ background and signal ($m_{\tilde{t}} = 400$ GeV, $m_{\tilde{\chi}_1^0} = 100$ GeV). We cut at $M_T(b_B, \not{E}_T) > 155$ GeV. The luminosity is 50 fb^{-1}.

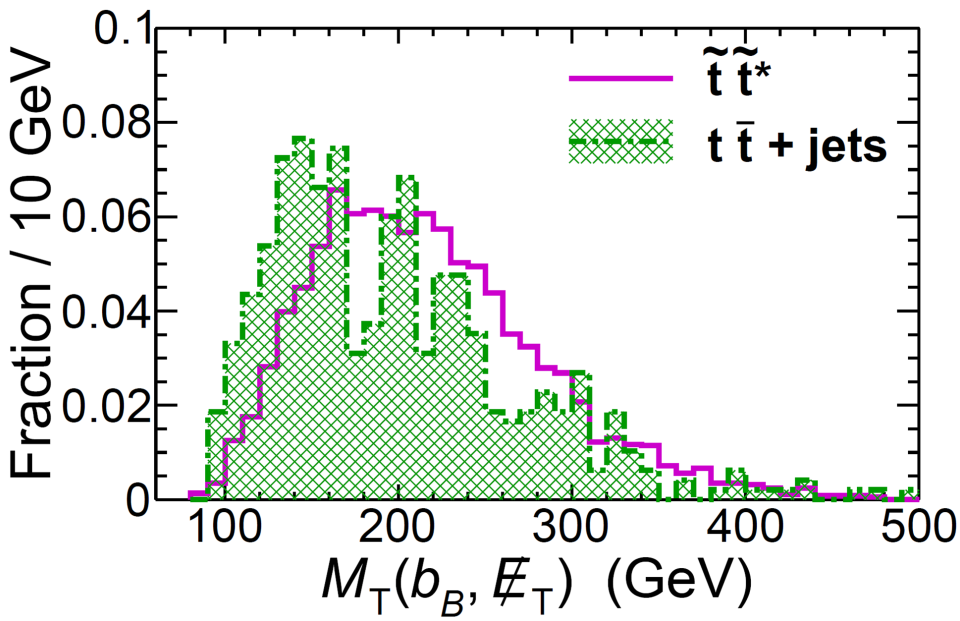

Table III.4: $M_T(b_B, \not{E}_T)$ cuts for various choices of masses. All masses are in GeV.

$\tilde{t}$	350	400	450	500	550	400	400
$\tilde{\chi}_1^0$	100	100	100	100	100	150	200
$M_T(b_B, \not{E}_T)$ cut	145	155	165	165	165	155	155

After the above cuts, we revert to the trijet $b_A j_A j_A$ in System A with similar angular cuts between missing energy and the b-tagged jet as will as no b-tagged jets. These angular cuts are efficient in reducing events with lost leptons. The cuts are chosen based on Figure III.5.

(iii) $\Delta\phi(b_A, \not{E}_T) > 1.2$ and $\Delta\phi(j_{A(1,2)}, \not{E}_T) > 0.7$, where $j_{A(1,2)}$ refer to the first and second leading jets in System A, respectively.

Figure III.5: Distributions of $\Delta\phi(b_A, \not{E}_T)$, $\Delta\phi(j_{A1}, \not{E}_T)$, and $\Delta\phi(j_{A2}, \not{E}_T)$ for $t\bar{t}$ background and signal ($m_{\tilde{t}} = 400$ GeV, $m_{\tilde{\chi}_1^0} = 100$ GeV). We cut at $\Delta\phi(b_A, \not{E}_T) > 1.2$, $\Delta\phi(j_{A(1,2)}, \not{E}_T) > 0.7$. Here, b_A, j_{A1} and j_{A2} denote the b, leading jet, and next leading jet of System A. The luminosity is 50 fb^{-1}.

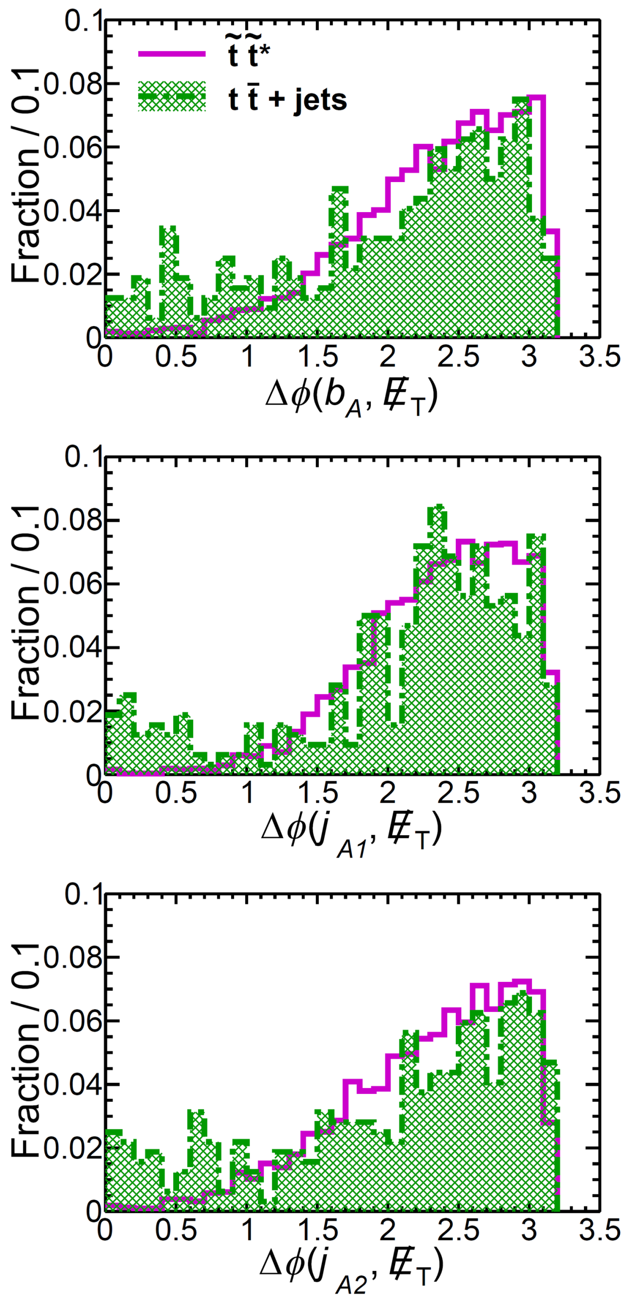

At a last step, M3 is applied in System B, followed by a W mass window cut on M2 (40 GeV $\leq$ M2 $\leq$ 120 GeV). The M3 distribution is shown in Figure III.6. Our final results with 110 GeV $\leq$ M3 $\leq$ 230 GeV are tabulated in Table III.5.

Figure III.6: Distribution of M3 in System B, after requiring 40 GeV $\leq$ M2 $\leq$ 120 GeV. Dispayed are: other sources of background (single top + jets, $W + n$ jets and $Z + n$ jets with $n \leq 6$, total background including $t\bar{t} + n$ jets and total background plus signal for our reference point ($m_{\tilde{t}} = 400$ GeV, $m_{\tilde{\chi}_1^0} = 100$ GeV). The luminosity is 50 fb^{-1}.

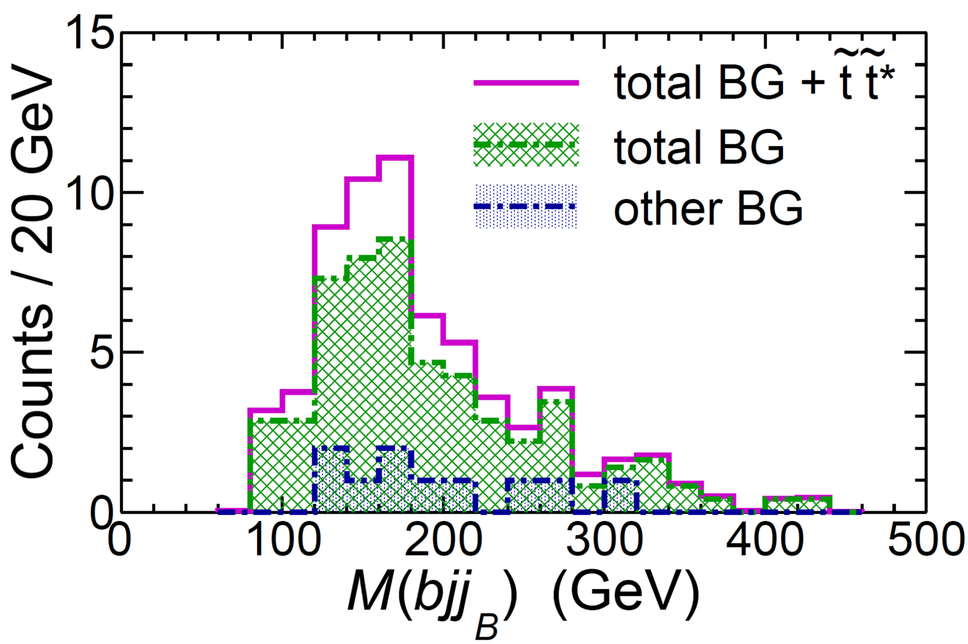

We note that for the point ($m_{\tilde{t}} = 350$ GeV, $m_{\tilde{\chi}_1^0} = 100$ GeV) we additionally impose $\Delta\phi(b_{A,B}, \not{E}_T) < 2.7$. Also, for the point ($m_{\tilde{t}} = 400$ GeV, $m_{\tilde{\chi}_1^0} = 200$ GeV), the W mass window cut on M2 of System B was taken as 60 GeV $\leq$ M2 $\leq$ 100 GeV, while the top quark mass window was taken as 140 GeV $\leq$ M3 $\leq$ 200 GeV.

Table III.5 and III.6 are a summary of the search performance for various choices of stop and neutralino masses.

Table III.5: Summary of effective cross sections (fb) for stop pair production and the SM background events in our stop search feasibility study. Masses and momenta are in GeV. Other sources of background include single top + jets, W + n jets and Z + n jets with $1 \leq n \leq 6$. The significance is given at 50 fb^{-1}.

$m_{\tilde{t}} = 350 \quad m_{\tilde{\chi}_1^0} = 100$	Signal	$t\bar{t} + n(\leq 2)$ jets	$t\bar{t} + n(\geq 3)$ jets	Others
Initial	760	2.0×10^5	0.24×10^5	2.8×10^6
Baseline Cuts (Section III.3.1)	9.96	192	147	31.7
$\not{E}_T > 145$ GeV	6.79	82.2	69.1	15.8
System A: M3 (Section III.3.2)	2.65	25.8	15.6	3.14
Angular and M_T cuts (Section III.3.3)	0.55	1.61	1.71	0.72
System B: M3 (Section III.3.4)	0.25	0.40	0.47	0.20
$\Delta\phi(b_{A,B}, \not{E}_T) < 2.7$	0.14	0.24	0.25	0.10
	Significance $(S/\sqrt{B})$ = 1.29			
$m_{\tilde{t}} = 400 \quad m_{\tilde{\chi}_1^0} = 100$	Signal	$t\bar{t} + n(\leq 2)$ jets	$t\bar{t} + n(\geq 3)$ jets	Others
Initial	337	2.0×10^5	0.24×10^5	2.8×10^6
Baseline Cuts (Section III.3.1)	5.55	192	147	31.7
$\not{E}_T > 170$ GeV	3.62	53.4	47.0	11.1
System A: M3 (Section III.3.2)	1.46	15.4	9.73	1.82
Angular and M_T cuts (Section III.3.3)	0.44	0.96	1.06	0.54
System B: M3 (Section III.3.4)	0.20	0.26	0.28	0.14
	Significance $(S/\sqrt{B})$ = 1.71			
$m_{\tilde{t}} = 450 \quad m_{\tilde{\chi}_1^0} = 100$	Signal	$t\bar{t} + n(\leq 2)$ jets	$t\bar{t} + n(\geq 3)$ jets	Others
Initial	160	2.0×10^5	0.24×10^5	2.8×10^6
Baseline Cuts (Section III.3.1)	2.52	192	147	31.7
$\not{E}_T > 195$ GeV	1.61	34.5	31.9	8.08
System A: M3 (Section III.3.2)	0.62	9.17	6.32	1.30
Angular and M_T cuts (Section III.3.3)	0.25	0.55	0.69	0.40
System B: M3 (Section III.3.4)	0.12	0.17	0.14	0.06
Significance $(S/\sqrt{B})$ = 1.39				
	Significance $(S/\sqrt{B})$ = 1.39			

Table III.5 Continued

$m_{\tilde{t}} = 500$ $m_{\tilde{\chi}_1^0} = 100$	Signal	$t\bar{t} + n(\leq 2)$ jets	$t\bar{t} + n(\geq 3)$ jets	Others
Initial	80.5	2.0×10^5	0.24×10^5	2.8×10^6
Baseline Cuts (Section III.3.1)	1.21	192	147	31.7
$\not{E}_T > 195$ GeV	0.86	34.5	31.9	8.08
System A: M3 (Section III.3.2)	0.32	9.17	6.32	1.30
Angular and M_T cuts (Section III.3.3)	0.15	0.55	0.69	0.40
System B: M3 (Section III.3.4)	0.07	0.17	0.14	0.06

Significance $(S/\sqrt{B}) = 0.81$

$m_{\tilde{t}} = 550$ $m_{\tilde{\chi}_1^0} = 100$	Signal	$t\bar{t} + n(\leq 2)$ jets	$t\bar{t} + n(\geq 3)$ jets	Others
Initial	43.0	2.0×10^5	0.24×10^5	2.8×10^6
Baseline Cuts (Section III.3.1)	0.57	192	147	31.7
$\not{E}_T > 195$ GeV	0.43	34.5	31.9	8.08
System A: M3 (Section III.3.2)	0.14	9.17	6.32	1.30
Angular and M_T cuts (Section III.3.3)	0.07	0.55	0.69	0.40
System B: M3 (Section III.3.4)	0.03	0.17	0.14	0.06

Significance $(S/\sqrt{B}) = 0.35$

$m_{\tilde{t}} = 400$ $m_{\tilde{\chi}_1^0} = 150$	Signal	$t\bar{t} + n(\leq 2)$ jets	$t\bar{t} + n(\geq 3)$ jets	Others
Initial	337	2.0×10^5	0.24×10^5	2.8×10^6
Baseline Cuts (Section III.3.1)	4.78	192	147	31.7
$\not{E}_T > 170$ GeV	2.76	53.4	47.0	11.1
System A: M3 (Section III.3.2)	1.01	15.4	9.73	1.82
Angular and M_T cuts (Section III.3.3)	0.23	0.96	1.06	0.54
System B: M3 (Section III.3.4)	0.11	0.26	0.28	0.14

Significance $(S/\sqrt{B}) = 0.94$

$m_{\tilde{t}} = 400$ $m_{\tilde{\chi}_1^0} = 200$	Signal	$t\bar{t} + n(\leq 2)$ jets	$t\bar{t} + n(\geq 3)$ jets	Others
Initial	337	2.0×10^5	0.24×10^5	2.8×10^6
Baseline Cuts (Section III.3.1)	3.34	192	147	31.7
System A: M3 (Section III.3.2)	1.13	67.2	38.8	7.40
Angular and M_T cuts (Section III.3.3)	0.87	45.8	28.3	6.04

Table III.5 Continued

$m_{\tilde{t}} = 400$	$m_{\tilde{\chi}_1^0} = 200$	Signal	$t\bar{t} + n(\leq 2)$ jets	$t\bar{t} + n(\geq 3)$ jets	Others
System B: M3 (Section III.3.4)		0.18	4.12	2.59	0.54
		Significance ($S/\sqrt{B}$) = 0.47			

Table III.6: Final significances for various choices of masses. All masses are in GeV. The luminosity is 50 fb^{-1}.

$\tilde{t}$	350	400	450	500	550	400	400
$\tilde{\chi}_1^0$	100	100	100	100	100	150	200
$S/\sqrt{B}$	1.29	1.71	1.39	0.81	0.35	0.94	0.47

CHAPTER IV

BINO-HIGGSINO DARK MATTER SCENARIO*

Due to small electroweak production the bounds on the neutralinos and charginos are much weaker. This sector, along with the sleptons, plays a crucial role in the dark matter physics of SUSY models. In the R-parity conserving minimal supersymmetric standard model, $\tilde{\chi}_1^0$ is typically the dark matter candidate. If $\tilde{\chi}_1^0$ is purely a Bino, its relic density tends to be large since the annihilation cross section is smaller than the required thermal annihilation rate $3 \times 10^{-26} cm^3/sec$. One way to obtain the correct relic density is to consider a thermal, well-tempered $\tilde{\chi}_1^0$ which is a mixture of Bino and Higgsino [23, 24, 25, 26, 27], while having $\tilde{\chi}_2^0$ and $\tilde{\chi}_3^0$ as primarily Higgsinos.

The purpose of this chapter is to probe the $\tilde{t}$ in a scenario with $\tilde{\chi}_1^0$ as a Bino-Higgsino mixture which satisfies the thermal dark matter relic density, and $\tilde{\chi}_{2,3}^0$ as mainly Higgsinos. All three are lighter than the top squark, which is in the sub-TeV range. The main theoretical motivation for considering a light top squark as well as light Higgsinos is naturalness, while the motivation of presence of a light Bino is to obtain the correct relic density for $\tilde{\chi}_1^0$, since if a sub-TeV $\tilde{\chi}_1^0$ is purely Higgsino, the relic density is too small [28, 29].

In such a scenario, $\tilde{t}$ mainly decays into $t\tilde{\chi}_{2,3}^0$ and $b\tilde{\chi}_1^\pm$ followed by $\tilde{\chi}_{2,3}^0 \to ll\tilde{\chi}_1^0$ via an intermediate slepton ("light selpton" case) or Z boson ("heavy slepton" case), and $\tilde{\chi}_1^\pm \to l\nu\tilde{\chi}_1^0$. The final state in $\tilde{t}\tilde{t}^*$ events has dileptons with jets and missing energy ($\not{E}_T$). We will consider both the light slepton case (slepton mass is between masses of $\tilde{\chi}_1^0$ and $\tilde{\chi}_2^0$) and the heavy slepton case (slepton mass is heavier than $\tilde{t}$) in events with at least two leptons, jets, and $\not{E}_T$.

The dilepton final states investigated in this chapter can lead to a quite robust $\tilde{t}$ search. The cross section for $\tilde{t}\tilde{t}^*$ production is appreciable at the LHC8 for the mass range between 300 and 700 GeV. In this chapter, I will show that the SUSY combinatoric and SM backgrounds are reduced by performing an opposite-sign same flavor (OSSF) minus opposite-sign different flavor (OSDF)

*Parts of this chapter are reprinted with permission from "*Top Squark Searches Using Dilepton Invariant Mass Distributions and Bino-Higgsino Dark Matter at the LHC*", by B. Dutta, T. Kamon, N. Kolev, K. Sinha, K. Wang, and S. Wu, Phys. Rev. D **87**, 095007 (2013), Copyright 2013 by The American Physical Society.

subtraction. The shape analysis of OSSF-OSDF dilepton mass distribution is done. If slepton masses are between $\tilde{\chi}_2^0$ and $\tilde{\chi}_1^0$, an edge in the dilepton mass distribution could be visible due to higher branching fractions of $\tilde{\chi}_{2,3}^0 \to ll\tilde{\chi}_1^0$ decays. This chapter is based on our work in [12].

IV.1 Benchmark Points

Mass spectra which satisfy the following mass relation are studied:

$$m_{\tilde{t}} > m_{\tilde{\chi}_3^0}, m_{\tilde{\chi}_2^0}, m_{\tilde{\chi}_1^\pm} > m_{\tilde{\chi}_1^0}, \tag{IV.1}$$

The possible $\tilde{t}$ decay modes are

$$\tilde{t} \to t\tilde{\chi}_1^0, \tag{IV.2}$$

$$\tilde{t} \to b\tilde{\chi}_1^\pm \to bl\bar{\nu}\tilde{\chi}_1^0 (\text{ or } bq\bar{q}'\tilde{\chi}_1^0), \tag{IV.3}$$

$$\tilde{t} \to b\tilde{\chi}_2^\pm \to bZ\tilde{\chi}_1^\pm. \tag{IV.4}$$

The leptons and quarks from the $\tilde{\chi}_1^\pm$ decays are through (off-shell) W bosons. Throughout this chapter, inclusion of charge conjugate modes is implied. The last mode is allowed when the $\tilde{\chi}_2^\pm$ is lighter than $\tilde{t}$.

In the light slepton case,

$$m_{\tilde{t}} > m_{\tilde{\chi}_3^0}, m_{\tilde{\chi}_2^0}, m_{\tilde{\chi}_1^\pm} > m_{\tilde{l}} > m_{\tilde{\chi}_1^0}, \tag{IV.5}$$

The leptons from the $\tilde{\chi}_3^0$ and $\tilde{\chi}_2^0$ decays are through sleptons.

$$\tilde{t} \to t\tilde{\chi}_{2,3}^0 \to tl^\pm\tilde{l}^{(*)\pm} \to tl^\pm l^\mp\tilde{\chi}_1^0. \tag{IV.6}$$

In the heavy slepton case,

$$m_{\tilde{l}} > m_{\tilde{t}} > m_{\tilde{\chi}_3^0}, m_{\tilde{\chi}_2^0}, m_{\tilde{\chi}_1^\pm} > m_{\tilde{\chi}_1^0}, \tag{IV.7}$$

The leptons from the $\tilde{\chi}_3^0$ and $\tilde{\chi}_2^0$ decays are through (off-shell) Z bosons.

$$\tilde{t} \to t\tilde{\chi}_{2,3}^0 \to tZ\tilde{\chi}_1^0 \to tl^\pm l^\mp\tilde{\chi}_1^0. \tag{IV.8}$$

In this Bino-Higgsino dark matter scenario, the final state of $\geq$ 2 jets + 2 leptons + $\not{E}_T$ events arises mostly from a combination of the $\tilde{t} \to b\tilde{\chi}_1^{\pm}$ and $\tilde{t} \to t\tilde{\chi}_{2,3}^0$ decays. The presence of a b-tagged jet in the final state is key to inferring the production of a third-generation squark. If both top squarks decay into a b and a $\tilde{\chi}_1^{\pm}$, then 2 b-tagged jets + 2 leptons + $\not{E}_T$ events are expected. It is clear that one obtains an edge in the dilepton invariant mass distribtuion as well as Z peak depending on the size of the $\mathcal{B}(\tilde{t} \to b\tilde{\chi}_2^{\pm})$ value.

The benchmark point in the light slepton case is displayed in Table IV.1.

Table IV.1: SUSY masses (in GeV) at "light slepton" benchmark point.

Particle	Mass (GeV)	$\mathcal{B}$
$\tilde{t}$	500	17%($t\tilde{\chi}_2^0$), 22%($t\tilde{\chi}_3^0$)
		8%($t\tilde{\chi}_1^0$), 53%($b\tilde{\chi}_1^{\pm}$)
$\tilde{\chi}_3^0$	176	88%($l\tilde{l}$)
$\tilde{\chi}_2^0$	175	100%($l\tilde{l}$)
$\tilde{\chi}_1^{\pm}$	164	22%($l\nu\tilde{\chi}_1^0$)
$\tilde{l}$	144	100%($l\tilde{\chi}_1^0$)
$\tilde{\chi}_1^0$	112	

In the heavy slepton case, the benchmark point has $m_{\tilde{t}} = 390$ GeV, with chargino and neutralinos similar to Table IV.1. SUSY masses at the benchmark point in the heavy slepton case are sown in Table IV.2.

Table IV.2: SUSY masses (in GeV) at "heavy slepton" benchmark point.

Particle	Mass (GeV)	$\mathcal{B}$
$\tilde{t}$	390	17%($t\tilde{\chi}_2^0$), 14%($t\tilde{\chi}_3^0$)
		7%($t\tilde{\chi}_1^0$), 62%($b\tilde{\chi}_1^{\pm}$)
$\tilde{\chi}_3^0$	175	7%($ll\tilde{\chi}_1^0$)
$\tilde{\chi}_2^0$	174	7%($ll\tilde{\chi}_1^0$)
$\tilde{\chi}_1^{\pm}$	164	22%($l\nu\tilde{\chi}_1^0$)
$\tilde{\chi}_1^0$	112	

We generate signal events with ISAJET + PYTHIA, followed by PGS4 detector simulation. The SM background of $t\bar{t} + (0-4)$ jets is generated using MadGraph [30] + PYTHIA + PGS4.

IV.2 Search Strategy

The analysis begins with selecting events with final states of $\geq$ 2 jets + $\geq$ 1 b-tagged jet + 2 leptons + large $\not{E}_T$. The following shows the detailed selection cuts:

(i) Exactly two isolated leptons (e or μ) with $p_T >$ 20 GeV and 10 GeV in $|\eta| < 2.5$, where the isolation is defined as $\sum p_T^{track} < 5$ GeV with $\Delta R = 0.4$;

(ii) At least two jets with $p_T > 30$ GeV in $|\eta| < 2.5$;

(iii) At least one b-tagged jet with $p_T > 30$ GeV in $|\eta| < 2.5$;

$\not{E}_T$ and H_T cuts are optimized for different benchmark points.

(iv) In the light slepton case, we choose $\not{E}_T > 150$ GeV; In the heavy slepton case, we choose $\not{E}_T > 190$ GeV;

(v) In the light slepton case, we choose $H_T > 100$ GeV; In the heavy slepton case, we choose $H_T > 180$ GeV.

At this stage, the dominant SM background is $t\bar{t}$ events. OSSF dileptons arising from the $\tilde{\chi}_2^0$ decay are kinematically correlated and its dilepton invariant mass distribution is expected to have an edge given by

$$M_{ll}^{edge} \sim m_{\tilde{\chi}_2^0} - m_{\tilde{\chi}_1^0}. \tag{IV.9}$$

The OSSF dilepton mass distribution from $t\bar{t}$ events can be modeled by the dilepton distribution of OSDF dilepton events [31]. The OSSF dilepton mass distribution from supersymmetric combinatoric background (i.e., uncorrelated leptonic pairs) can also be modeled by OSDF dilepton mass distribution. This leads us to adopting subtracting OSDF distribution from OSSF distribution. The light slepton benchmark events would arise in an excess in OSSF-OSDF dilepton mass distribution.

IV.3 Results

In this section, the $\not{E}_T$ and H_T cuts will be optimized and applied to reduce the background. We will list our signal and background at different stages of cuts and flavor subtraction. The final significance at 30 fb^{-1} of 8 TeV LHC is calculated. We achieve the final expected experiment reach and exclusion of $m_{\tilde{t}}$. It is shown that a small value of $\mathcal{B}(Z \to ll)$ causes smaller significance in the heavy slepton case compared to the light slepton case.

IV.3.1 Results in Light Slepton Case

The OSDF dilepton mass distribution for the SUSY benchmark point in Table IV.1 along with the SM $t\bar{t} + (0-4)$ jets background is shown in the shaded histogram in Figure IV.1, while its OSSF distribution (blank histogram) is overlaid. A clear edge is seen at around 63 GeV for 30 fb^{-1} luminosity.

Figure IV.1: The dilepton invariant mass distributions for $t\bar{t} + (0-4)$ jets background and the benchmark point in Table IV.1 are displayed for 30 fb^{-1} luminosity. The unshaded historgram shows the M_{ll}^{OSSF} distribution, while the shaded historgram shows the M_{ll}^{OSDF} distribution, which is fitted with the dot-dashed curve. The solid curve shows the subtracted M_{ll}^{diff} distribution.

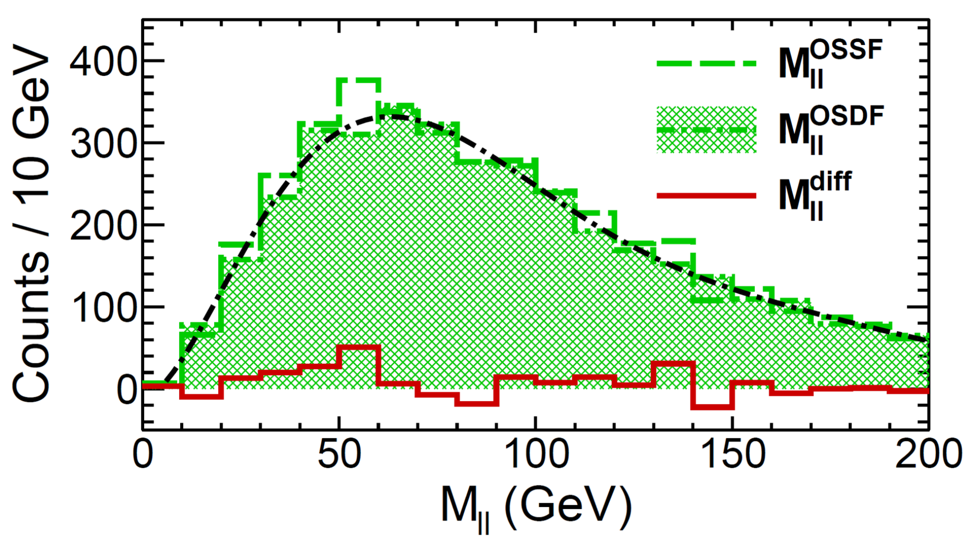

The excess in OSSF-OSDF dilepton mass distribution for this benchmark mass point is evaluated in terms of significances ($\mathcal{S}$) in Table IV.3. Here $\mathcal{S} = N_S/\sqrt{N_S + N_B}$, where N_B is determined by fitting the entire (SUSY plus $t\bar{t}$) OSDF dilepton distribution to a polynomial function curve and counting the number of events under this curve in the excess range of 20 GeV $< M_{ll} <$ 70 GeV. N_S is the number of OSSF dilepton events in excess above N_B within this range.

In Figure IV.2, we fix values of $m_{\tilde{t}} = 500$ GeV, $m_{\tilde{\chi}_1^0} = 112$ GeV, and $m_{\tilde{\chi}_3^0} \sim m_{\tilde{\chi}_2^0}$, as is shown in Table IV.1. Then by varying $m_{\tilde{\chi}_2^0}$, the flavor subtracted distributions at $\Delta M = m_{\tilde{\chi}_2^0} - m_{\tilde{\chi}_1^0} =$ 53, 63, 70, 77, and 100 GeV are shown. The dilepton mass distribution edge for all these mass differences except $\Delta M = 100$ GeV can be seen clearly. Positions of edges are shifted due to the changing of the mass difference between $\tilde{\chi}_2^0$ and $\tilde{\chi}_1^0$. For $\Delta M = 100$ GeV, the signal acceptance is lower and the dilepton study does not have sensitivity at 30 fb^{-1} luminosity.

Figure IV.2: The subracted dilepton invariant mass distribution M_{ll}^{diff} as $\Delta M = m_{\tilde{\chi}_2^0} - m_{\tilde{\chi}_1^0}$ is varied, for $m_{\tilde{t}} = 500$ GeV and $m_{\tilde{\chi}_1^0} = 112$ GeV for 30 fb^{-1} luminosity.

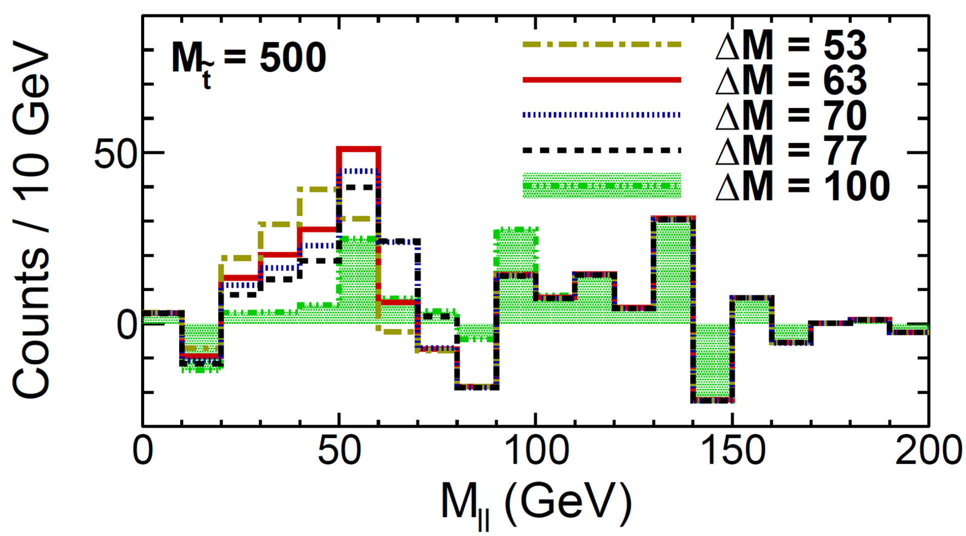

In Figure IV.3, we fix the mass difference between $\tilde{\chi}_2^0$ and $\tilde{\chi}_1^0$ to be 63 GeV (with $m_{\tilde{\chi}_1^0} = 112$ GeV and $m_{\tilde{\chi}_3^0} \sim m_{\tilde{\chi}_2^0} = 175$ GeV at the benchmark values in Table IV.1). Then by varying the $m_{\tilde{t}}$, the flavor subtracted distributions for $t\bar{t} + (0-4)$ jets background plus signal events for $m_{\tilde{t}} =$ 390, 440, 500, 550, and 600 GeV are shown. An edge in the dilepton invariant mass distribution can be seen around $\Delta M = 63$ GeV. The excess drops with the increasing of the stop mass. The edge for $m_{\tilde{t}}$ upto to 550 GeV can be distinguished from the background for 30 fb^{-1} luminosity.

Figure IV.3: The subtracted dilepton invariant mass distribution M_{ll}^{diff} as the $\tilde{t}$ mass is varied, all other masses remain at the benchmark value in Table IV.1 for 30 fb^{-1} luminosity.

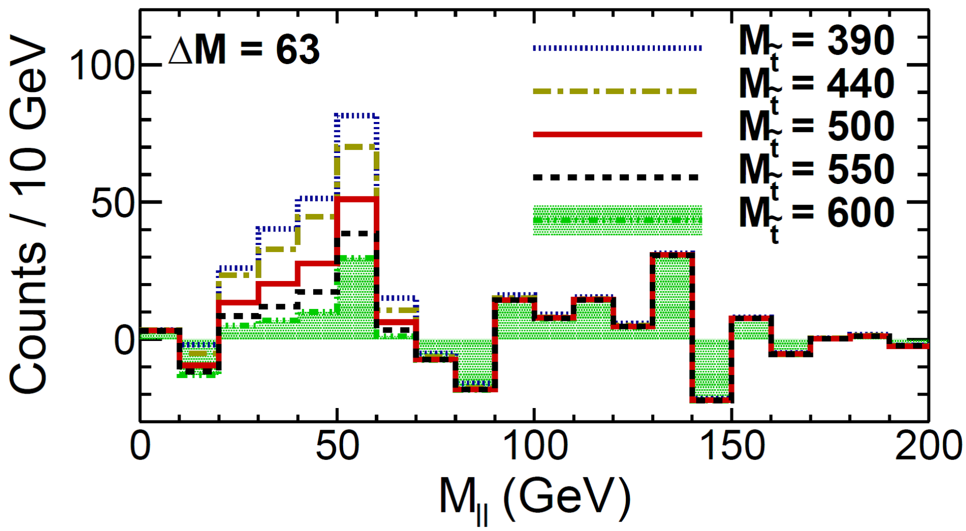

Table IV.3 shows the significances for different top squark masses at 30 fb^{-1} luminosity in cases where at least one of the jets is required to be a b-tagged jet. The significance of the benchmark scenario for $m_{\tilde{t}} = 500$ GeV is above 3σ for 30 fb^{-1} luminosity. As the top squark mass increases, the production cross sections decreases which leads to smaller significances.

Table IV.3: (Light slepton case) Signal and background cross sections in fb for various $\tilde{t}$ masses with $m_{\tilde{\chi}_1^0} = 112$ GeV and $m_{\tilde{\chi}_{2,3}^0} = 175$ GeV. Significances ($\mathcal{S}$) are given at 30 fb^{-1} luminosity.

$\tilde{t}$ mass (GeV)	Signal	Background	$\mathcal{S}$ ($\geq$ 1b)
390	7.08	46.4	5.3
440	6.00	45.6	4.6
500	3.90	45.1	3.1
550	2.60	44.9	2.1
600	1.70	44.8	1.4

IV.3.2 Results in Heavy Slepton Case

In this section, we discuss the results in the heavy slepton case. Table IV.4 shows signal and background cross sections at different stages of cuts and flavor subtraction for the benchmark point listed in IV.2. The final significance at 30 fb^{-1} luminosity is 1.7 if a b jet is required in the event sample. A small value of $\mathcal{B}(Z \to ll)$ causes smaller significance in the heavy slepton case compared to the light slepton case.

Table IV.4: (Heavy slepton case) Cross section (fb) for signal and background at different stages of event selection and flavor subtractions are shown for the benchmark point in Table IV.2.

Event selection	$\tilde{t}\tilde{t}^*$	$t\bar{t} + jets$
$N_l \geq 2$, $N_j \geq 2$, $N_b \geq 1$, $\not{E}_T > 190$ GeV, $H_T > 180$ GeV	2.1	84.7
OSSF dileptons with 20 GeV $< M_{ll}^{OSSF} <$ 70 GeV	0.70	13.2
OSDF dileptons with 20 GeV $< M_{ll}^{OSDF} <$ 70 GeV	0.44	12.8
OSSF-OSDF dileptons with 20 GeV $< M_{ll}^{OSSF-OSDF} <$ 70 GeV	0.26	0.40

CHAPTER V

COMPRESSED SCENARIO

The challenge of investigating $\tilde{t}$ pair production lies in the huge background from top quark pair production. For this decay topology, the particles in the final state are identical to the $t\bar{t}$ background supplemented with missing transverse energy ($\not{E}_T$). The challenge is exacerbated when the mass gap between $\tilde{t}$ and $\tilde{\chi}_1^0$ is small. The $m_{\tilde{t}} - m_{\tilde{\chi}_1^0} = m_t$ line on the $m_{\tilde{t}} - m_{\tilde{\chi}_1^0}$ plane is a virtual Rubicon, and current exclusion bounds are non-existent near it.

In this compressed scenario ($\Delta m = m_{\tilde{t}} - m_{\tilde{\chi}_1^0} \sim m_t$), search strategies that rely on $\not{E}_T$ to reduce $t\bar{t}$ background have poor performance. The challenge is even greater when $\tilde{\chi}_1^0$ becomes vanishingly small in the compressed region, so that $m_{\tilde{t}} \sim m_t$. In this case, the $\not{E}_T$ discrimination between signal and background becomes very ineffective.

The purpose of this chapter is to propose the search strategy for $\tilde{t}$ pairs in the compressed scenario using Vector Boson Fusion (VBF) topology selection. We point out that the VBF topology can be exploited in probing compressed top squark scenario. The requirement of two energetic jets in the forward region with large dijet invariant mass is very effective in reducing SM backgrounds. In contrast to other $\tilde{t}$ searches where compressed spectrum results in low $\not{E}_T$, making it difficult to discriminate against $t\bar{t}$ background, VBF topology searches naturally give rise to larger $\not{E}_T$ since the momentum of the particles centrally produced in the $\tilde{t}$ system must balance the high p_t of the scattered partons. Thus, in the compressed scenario, the $\tilde{\chi}_1^0$ resulting from the $\tilde{t}$ decay can carry significant $\not{E}_T$, providing better control of the $t\bar{t}$ background. However, for small Δm, the p_T of b-jets becomes soft, which makes b-jet identification challenging; consequently, the signal significance starts reducing.

The $\tilde{\chi}_1^0$ in our studies is mostly Bino, while the $\tilde{t}$ is mostly $\tilde{t}_R$ such that the dominant decay mode of the $\tilde{t}$ is $\tilde{t} \to t\tilde{\chi}_1^0$, or $\tilde{t} \to bW\tilde{\chi}_1^0$. In the following sections, we will perform this study at LHC14. In the case where the mass difference between stop and the lightest neutralino is slightly greater than the mass of the top quark (we call it "two-body decay" case), stop does the 2-body decay of a top quark, and the lightest neutralino. In the case where the mass difference between stop and the lightest neutralino is smaller than the mass of top quark (we call it "three-body decay" case), stop does the 3-body decay of a bottom quark, a W boson and the lightest neutralino. Both cases will be studied. The strategy and results we show in this chapter are firstly presented in our work [13].

V.1 Benchmark Points

In the two-body decay case, $\tilde{t} \to t\tilde{\chi}_1^0$. We choose the benchmark points with $\tilde{t}$ masses in the range of 300-600 GeV, and keeping $\Delta m \sim m_t + 7$ GeV. Some points are $(m_{\tilde{t}}, m_{\tilde{\chi}_1^0})$ = (300, 120) GeV, (400, 220) GeV, and (500, 320) GeV, and listed in V.1. The other colored particles, neutralinos and charginos are assumed to be much heavier.

In the three-body decay case, $\Delta m = m_{\tilde{t}} - m_{\tilde{\chi}_1^0} < m_t$ and $\tilde{t} \to bW\tilde{\chi}_1^0$. We note that in this mode 85 GeV $\leq \Delta m \leq$ 172 GeV. Probing this three-body decay mode presents even severe challenges. The challenges for small $\Delta m \sim$ 85 GeV are lack of $\not{E}_T$ (near the compressed limit, the $\tilde{\chi}_1^0$ provides little transverse missing energy) and the softness of the final state b-jets, which makes b-identification difficult. For larger $\Delta m \sim$ 172 GeV, the signal looks like the $t\bar{t}$ background and the challenges are similar to the ones encountered in probing the compressed regions of the two-body decay mode.

The benchmark point we choose in the three-body decay case have $\tilde{t}$ masses in the range of 250-400 GeV. For the same $\tilde{t}$ mass, within the range allowed for three-body decay mode several different values of $\tilde{\chi}_1^0$ and hence Δm are chosen. Some points are $(m_{\tilde{t}}, m_{\tilde{\chi}_1^0})$ = (250, 85) GeV, (300, 135) GeV, (400, 235) GeV, and (300, 150) GeV, and listed in V.2. The other supersymmetric particles are assumed to be much heavier.

Signal and background samples are generated with MADGRAPH followed by the parton showering and hadronization with PYTHIA and the detector simulation using PGS4.

V.2 Search Strategy

For this feasibility study, inclusive $\tilde{t}\tilde{t}^*+$ jets samples are generated. The study is performed in the $2j + 1l + 2b + \not{E}_T$ final state. The search strategy is based on three steps. First, we use the unique features of VBF topology to reduce V + jets backgrounds (where V is either W or Z). Second, we use decay properties of the centrally produced $\tilde{t}$ pair, namely the requirement of an isolated lepton and two b-tagged jets from top quarks, to further reduce light quark QCD backgrounds and other channels that are also produced by VBF processes. Finally, the $\not{E}_T$ cut is optimized for each choice of $(m_{\tilde{t}}, m_{\tilde{\chi}_1^0})$.

The following event selections are applied:

(i) VBF topology selection: the events are required to have the presence of at least two jets (j_1, j_2) satisfying: (1) $p_T(j_1) \geq 75$ GeV $p_T(j_2) \geq 50$ GeV in $|\eta| \leq 4$; (2) $\eta_{j_1}\eta_{j_2} < 0$; (3) $|\Delta\eta(j_1 j_2)| > 4.2$; (4) dijet invariant mass $M_{j_1 j_2} > 500$ GeV. This reduces the W+jets and Z+jets backgrounds.

(ii) One isolated lepton with $p_T \geq 20$ GeV is required.

(iii) Two loosely b-tagged jets with $p_T \geq 30$ GeV in $|\eta| < 2.5$ are required. The b-jet identification efficiency and fake rate are taken to be 70% and 1%, respectively.

(iv) The big $\not{E}_T$ requirement. A different $\not{E}_T$ requirement is used for each different top squark mass point.

V.3 Results

In this section, the $\not{E}_T$ cuts are optimized for each different top squark mass point to reduce the background. We will list the signal and background cross sections at different stages of cuts flow. Significance will be calculated at luminosity 300, 1000, and 3000 fb^{-1} of 14-TeV LHC for both two-body decay case and three-body decay case.

V.3.1 Results in Two-body Decay Case

In the two-body decay case, $\not{E}_T$ cuts are chosen to be $\not{E}_T > 50$ GeV for $(m_{\tilde{t}}, m_{\tilde{\chi}_1^0}) = (300, 120)$ GeV point, $\not{E}_T > 100$ GeV for $(m_{\tilde{t}}, m_{\tilde{\chi}_1^0}) = (400, 220)$ GeV, and $\not{E}_T > 150$ GeV for $(m_{\tilde{t}}, m_{\tilde{\chi}_1^0}) = (500, 320)$ GeV. The cut flow table with corresponding cross-sections at each stage are shown in table V.1 for the benchmark points of $(m_{\tilde{t}}, m_{\tilde{\chi}_1^0}) = (300, 120)$ GeV and (400, 220) GeV. The VBF topology selection and $\not{E}_T$ cuts are very effective in improving the signal to background ratio.

Figure V.1 shows the distributions of $\not{E}_T$ before and after the VBF topology selection. The $\not{E}_T$ distribution before (blue diagonally dashed histogram) and after (green horizontally dashed histogram) VBF topology selections for the benchmark point with $m_{\tilde{t}} = 400$ GeV, $m_{\tilde{\chi}_1^0} = 220$ GeV

Table V.1: (Two-body decay case) Summary of the effective cross sections (fb) for different benchmark signal points as well as the $t\bar{t}$ background at LHC14. Masses and momenta are in GeV.

$(m_{\tilde{t}}, m_{\tilde{\chi}_1^0})$	Selection	Signal	$t\bar{t}$ + jets
(300, 120)	VBF topology selection	95.7	16774
	1 lepton	22.1	3587
	2 b-jets	9.70	1612
	$\not{E}_T > 50$	8.00	924
(400, 220)	VBF topology selection	25.2	16774
	1 lepton	5.93	3587
	2 b-jets	2.84	1612
	$\not{E}_T > 100$	1.48	337
(500, 320)	VBF topology selection	7.50	16774
	1 lepton	1.69	3587
	2 b-jets	0.74	1612
	$\not{E}_T > 150$	0.27	123

are shown overlaid with the $t\bar{t}$ + jets background (red diagonally dashed histogram). From the figure, it is clear that a large $\not{E}_T$ cut is needed to reduce the background.

The significance $\mathcal{S} = N_S/\sqrt{N_S + N_B}$, where N_S and N_B are the signal and background rates, respectively, is plotted in Figure V.2 as a function of $m_{\tilde{t}}$, keeping $\Delta m = m_{\tilde{t}} - m_{\tilde{\chi}_1^0} \sim m_t + 7$ GeV, for 200, 1000 and 3000 fb^{-1} of integrated luminosity at LHC14. We find that compressed scenarios with $m_{\tilde{t}} \sim 390$ GeV (340 GeV) can be probed at 3σ (5σ) level with 1000 fb^{-1} of integrated luminosity. The reach increases to 440 GeV (390 GeV) at 3σ (5σ) for 3000 fb^{-1} of luminosity.

V.3.2 Results in Three-body Decay Case

In the three-body decay case, we also notice that the optimization of $|\Delta(j_1 j_2)\eta|$ and low threshold of b-jets are helpful to improve the significance. We use $|\Delta\eta(j_1 j_2)| > 3.5$ and $p_T \geq 20$ GeV for b-jets in this case. We also optimize the $\not{E}_T$ requirement for each different $(m_{\tilde{t}}, m_{\tilde{\chi}_1^0})$ point. The $\not{E}_T$ cuts are chosen to be $\not{E}_T > 100$ GeV for $(m_{\tilde{t}}, m_{\tilde{\chi}_1^0}) = (300, 150)$ GeV and $\not{E}_T > 200$ GeV for (400, 235) GeV.

The cut flow table with corresponding cross sections at each stage is shown in Table V.2 for the

Figure V.1: (Two-body decay case) Distributions normalized to unity of $\not{E}_T$ before (blue diagonally dashed histrogram) and after (green horizontally dashed histogram) VBF tagging selections for signal overlaid with $t\bar{t}$ + jets background (red diagonally dashed histogram) for the benchmark point with $m_{\tilde{t}} = 400$ GeV, $m_{\tilde{\chi}_1^0} = 220$ GeV.

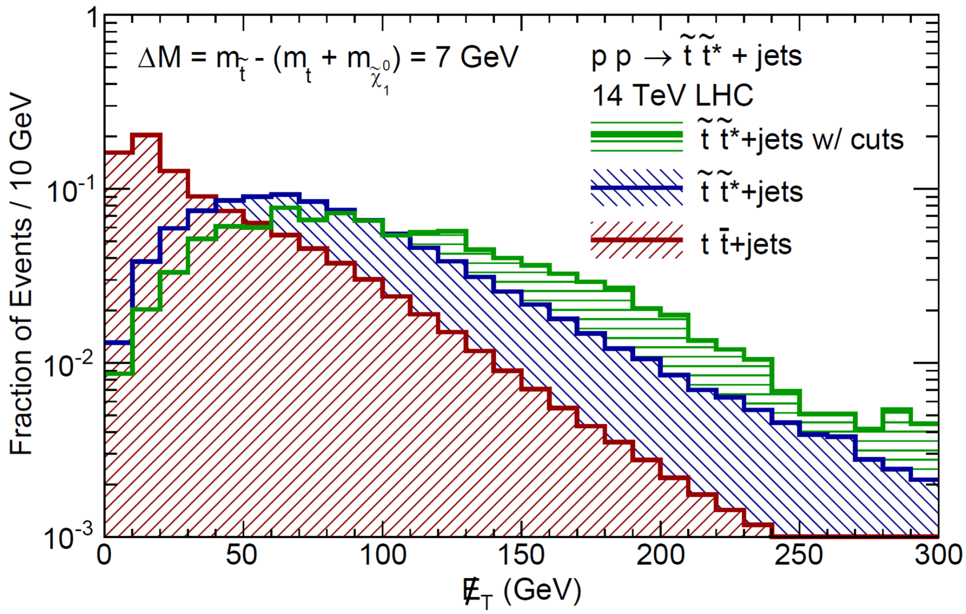

benchmark points of $(m_{\tilde{t}}, m_{\tilde{\chi}_1^0})$ = (250, 85) GeV, (300, 135) GeV, and (400, 235) GeV, corresponding to $\Delta m = 165$ GeV, and $(m_{\tilde{t}}, m_{\tilde{\chi}_1^0})$ = (300, 150) GeV, corresponding to $\Delta m = 150$ GeV.

From the table V.2 we find that large $\not{E}_T$ is very useful to reduce the background. Also, as Δm increases, the b jet becomes more energetic and the signal rate improves. We show this feature explicitly by choosing $m_{\tilde{t}} = 300$ GeV and $m_{\tilde{\chi}_1^0} = 150$ and 135 GeV. We note that b-jet identification is an important issue for this decay mode, in our analysis as well as other analysis which does not rely on VBF topology selection.

Figure V.3 shows the distributions of $\not{E}_T$ normalized to unity for signal (green horizontally dashed histogram) and $t\bar{t}$ + jets background (red diagonally dashed histogram) after VBF topology selection and lepton and b-jet requirements for the benchmark point with $m_{\tilde{t}} = 300$ GeV, $m_{\tilde{\chi}_1^0} = 135$ GeV. From the figure, it is clear that a large $\not{E}_T$ cut is needed to reduce the background.

Figure V.4 shows the p_T distribution of the two b-jets for the point $(m_{\tilde{t}}, m_{\tilde{\chi}_1^0})$ = (300, 165) GeV. As Δm decreases, p_T decreases which is shown in Figure V.5. This Figure highlights the importance

Table V.2: (Three-body decay case) Summary of the effective cross sections (fb) for different benchmark signal points as well as the $t\bar{t}$ background at LHC14. Masses and momenta are in GeV.

$(m_{\tilde{t}}, m_{\tilde{\chi}_1^0})$	Selection	Signal	$t\bar{t}$ + jets
	VBF topology selection	465.6	38787.8
(250, 85)	1 lepton	93.5	8107.9
$\Delta m = 165$ GeV	2 b-jets	25.3	3096.0
	$\not{E}_T > 100$	12.9	682.5
	VBF topology selection	217.9	38787.8
(300, 135)	1 lepton	42.8	8107.9
$\Delta m = 165$ GeV	2 b-jets	11.5	3096.0
	$\not{E}_T > 100$	6.7	682.5
	VBF topology selection	50.6	38787.8
(400, 235)	1 lepton	10.3	8107.9
$\Delta m = 165$ GeV	2 b-jets	2.76	3096.0
	$\not{E}_T > 200$	1.92	****
	VBF topology selection	194.2	38787.8
(300, 150)	1 lepton	39.9	8107.9
$\Delta m = 150$ GeV	2 b-jets	8.09	3096.0
	$\not{E}_T > 100$	5.00	682.5

Figure V.2: (Two-body decay case) Significance as a function of $m_{\tilde{t}}$, keeping $\Delta m = m_{\tilde{t}} - m_{\tilde{\chi}_1^0} \sim m_t + 7$ GeV. The black, red and green curves show the significance for integrated luminosities of 300, 1000, and 3000 fb^{-1}, respectively at LHC14. The horizontal lines denote 3σ and 5σ significance, respectively.

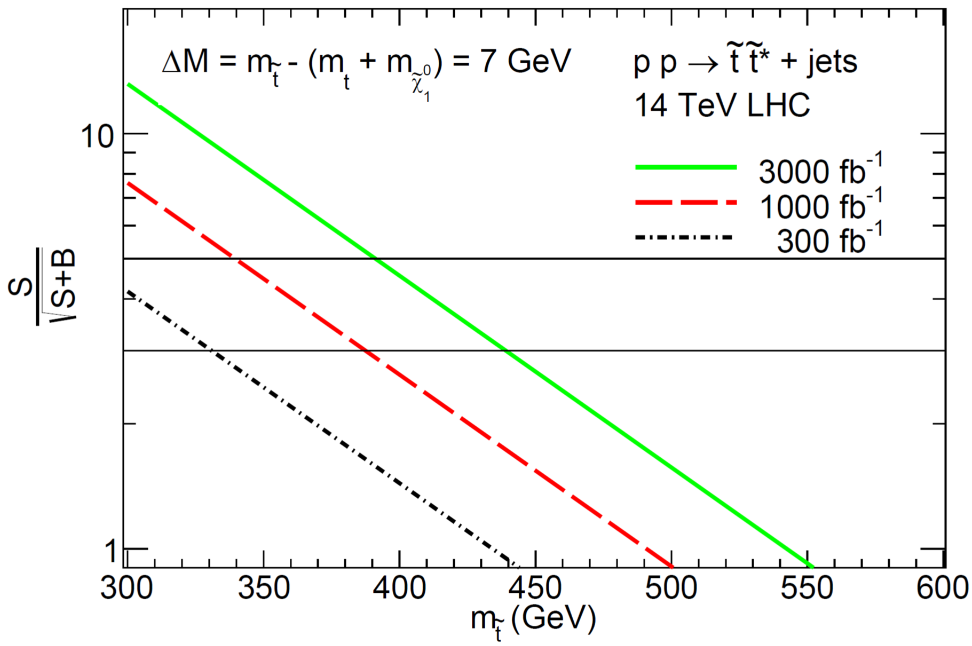

of having efficient and robust b-tagging at low p_T (~ 20 GeV) in order to maintain sensitivity to compressed (small Δm) scenarios. The CMS and ATLAS experiments have shown the ability to identify b-jets down to p_T of approximately 20 GeV with the 8 TeV data [32]. However, the challenge of identifying low p_T b-jets is expected to increase significantly under the harsh pileup conditions of the 14 TeV LHC. Preliminary CMS detector upgraded studies have shown the ability to efficiently identify b-jets down to $p_T = 30$ GeV [33] and we take this opportunity to request the experiments to continue to study the possibility of maintaining robust and efficient b-tagging down to 20 GeV.

As an example, for the benchmark point of Figure V.5, the expected signal rate decreases by 50% if the b-jet p_T threshold is increased from 20 to 30 GeV (assuming similar b-tagging efficiency down to 20 GeV). As expected this decrease in signal rate becomes more pronounced as Δm becomes smaller.

Figure V.3: (Three-body decay case) Distributions of $\not{E}_T$ normalized to unity for signal (green horizontally dashed histogram) and $t\bar{t}$ + jets background (red diagonally dashed histogram) after VBF tagging selections and lepton and b-jet requirements for the benchmark point with $m_{\tilde{t}} = 300$ GeV, $m_{\tilde{\chi}_1^0} = 135$ GeV.

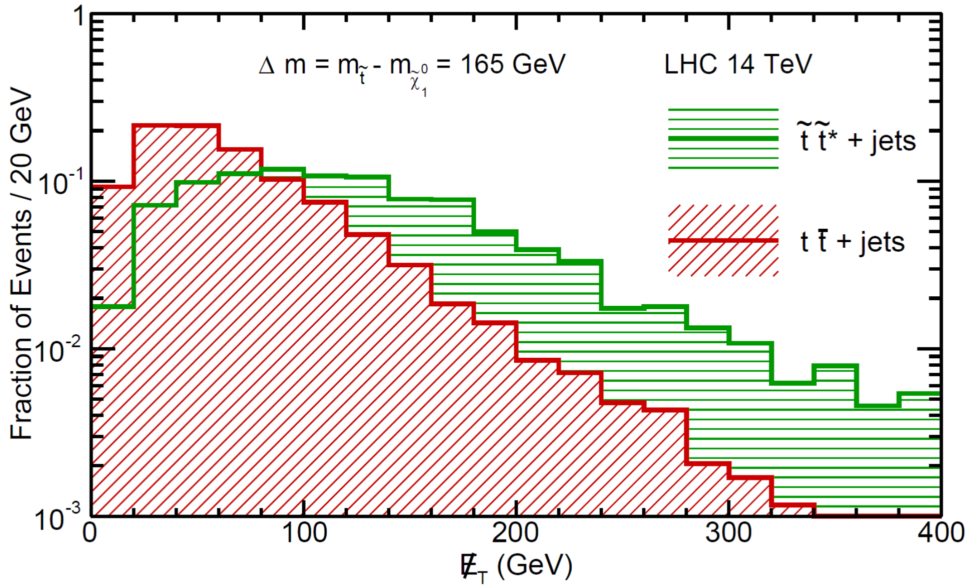

The significance $\mathcal{S}$ is plotted in Figure V.6 as a function of $m_{\tilde{t}}$, keeping $\Delta m = 165$ GeV, for 300, 1000 and 3000 fb^{-1} of integrated luminosities at LHC14. The reach for $\tilde{t}$ is 275 (300) GeV at 5σ (3σ) with 300 fb^{-1} and 340 (370) GeV at 5σ (3σ) with 3000 fb^{-1} integrated luminosity.

Figure V.4: (Three-body decay case) Distributions of p_T of the two b-jets for the benchmark point with $m_{\tilde{t}} = 300$ GeV, $m_{\tilde{\chi}_1^0} = 135$ GeV.

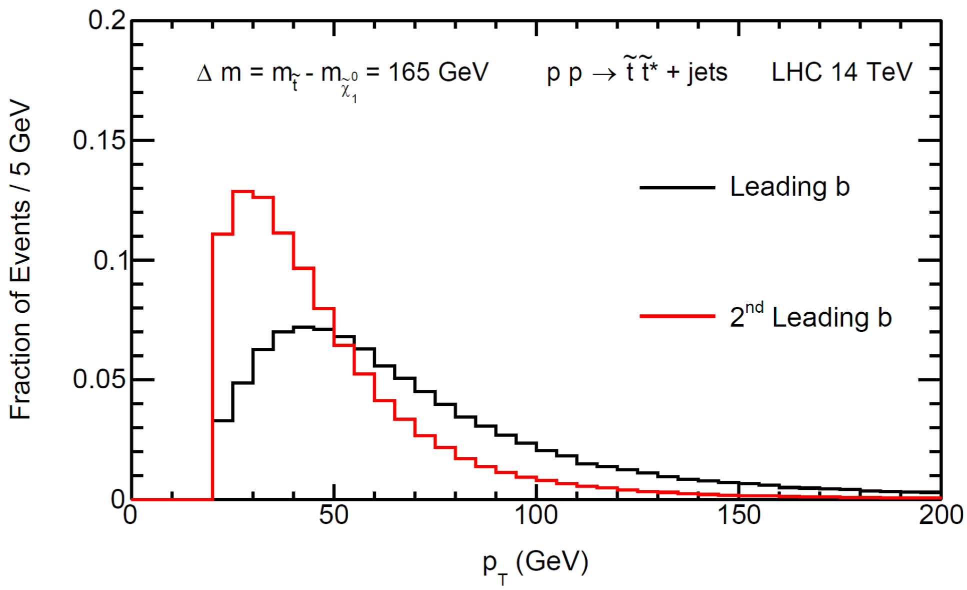

Figure V.5: (Three-body decay case) Distributions of p_T of the two b-jets for the benchmark point with $m_{\tilde{t}} = 300$ GeV, $m_{\tilde{\chi}_1^0} = 175$ GeV.

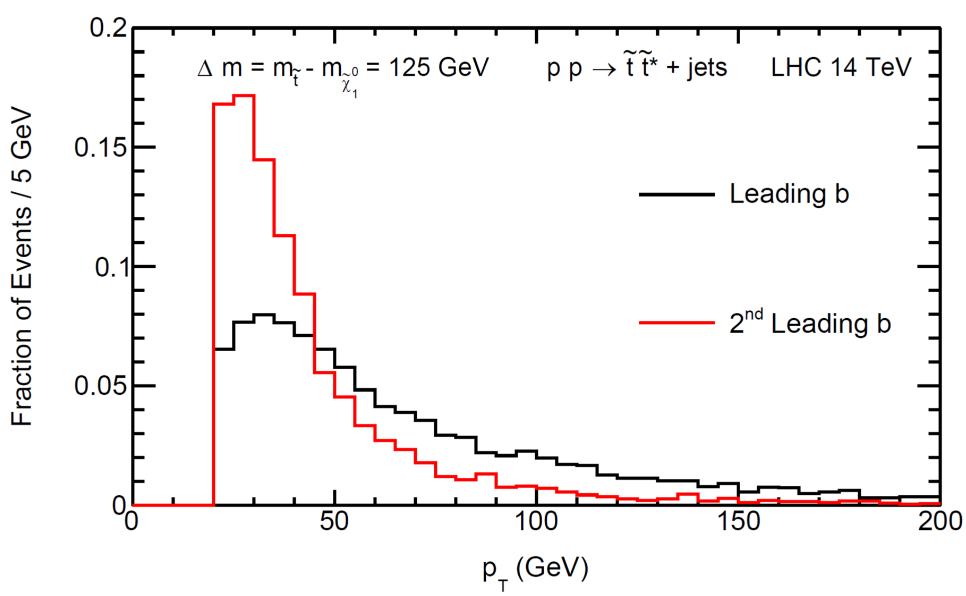

Figure V.6: (Three-body decay case) Significace as a function of $m_{\tilde{t}}$, keeping $\Delta m = m_{\tilde{t}} - m_{\tilde{\chi}_1^0} \sim$ 165 GeV for integrated luminosities of 300, 1000, and 3000 fb^{-1} at LHC14.

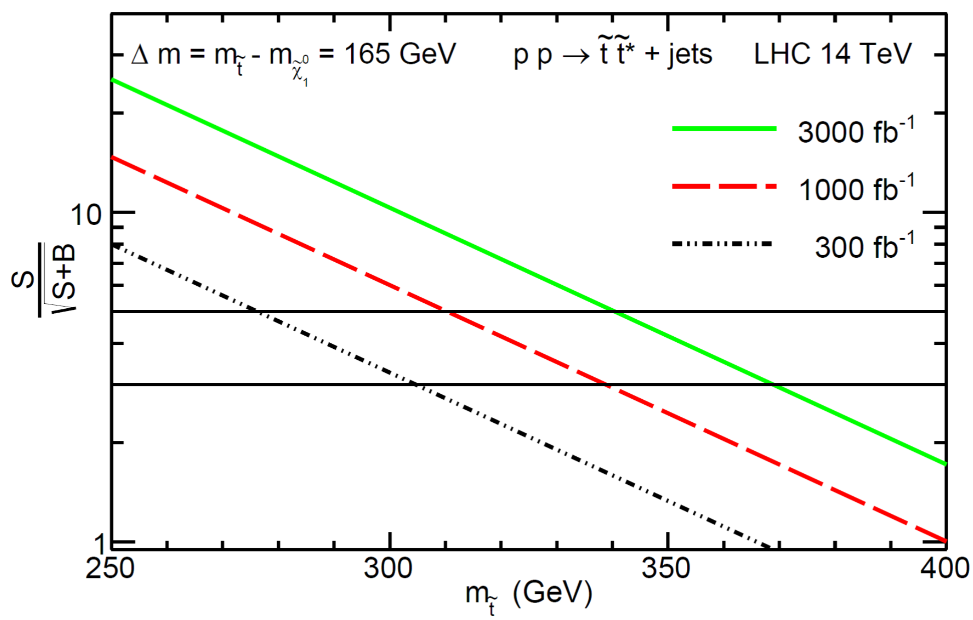

CHAPTER VI

SUMMARY AND CONCLUSION

Due to its importance in stabilizing the Higgs mass, probing the $\tilde{t}$ is a high-priority study at the LHC. This dissertation describes the search strategies we developed for the lighter top squark at the LHC. Both the production from the cascade decay of gluino and squark, and the direct production of stop pairs ($\tilde{t}\tilde{t}^*$) are investigated.

When $\tilde{t}$ is produced from the cascade decay of gluino and squark, we determine stop mass through endpoint measurements of kinematic observables arising from cascade decay. We perform the analysis in the case where the lightest neutralino $\tilde{\chi}_1^0$ is mostly Bino and next lightest neutralino $\tilde{\chi}_2^0$ is mostly Wino, the Higgsino components are negligible. The dark matter relic density is satisfied by the coannihilation mechanism. The stop-neutralino ($\tilde{t} \sim \tilde{\chi}_1^0$) coannihilation scenario is considered. In this scenario, the relevant decay chain associated with the dominant production process for the reconstruction of third generation squarks is $\tilde{g} \to \tilde{b} + b \to \tilde{t} + W + b \to \tilde{\chi}_1^0 + c + W + b$.

Our search strategy in such scenario relies on the construction of kinematic observables using endpoint technique, since these are a particularly sharp tool for such diagnosis. We constructed two new observables, M_{jW}^{end} and M_{bW}^{end}, to determine the masses of the $\tilde{t}$ and $\tilde{b}$. The determination of the $\tilde{t}$ and $\tilde{b}$ masses is especially challenging, since both decay to b quarks. To make the problem worse, stop decays to missing energy by emitting a low energy jet in this coannihilation scenario. The BEST technique is applied to get rid of background. We showed how to reconstruct the stop mass for a light gluino mass point. Our strategy works well at benchmark points with heavier mass spectrum, as preferred by current LHC data. We show the results for a benchmark point with heavy gluino mass ($m_{\tilde{g}} \sim 1.2$ TeV). In such case, higher luminosity is required to obtain endpoints.

When the lighter top squarks are produced from the direct production processes of stop pairs, we considered three scenarios.

In the fully hadronic final state scenario, we have explored a search strategy for a light stop, using M3 variable in the fully hadronic channel. The gluino and the first two generation squarks are assumed to be too heavy to be produced significantly at the LHC. Searches are carried out in the case where $\tilde{\chi}_1^0$ is mainly a Bino and $\tilde{\chi}_2^0$ is mainly a Wino. In such scenario, The dominant decay chain we considered is $pp \to \tilde{t}\tilde{t}^* \to (t\tilde{\chi}_1^0)(\bar{t}\tilde{\chi}_1^0) \to (bjj\tilde{\chi}_1^0)(\bar{b}jj\tilde{\chi}_1^0)$.

We fist performed $M3^{min}$ to identify a top quark system (System A). Next, we performed M3 again to identify the second top quark (System B), along with a series of kinematical cuts to reduce the SM backgrounds. Throughout the study, we used PGS4 detector simulation and considered W + n jets, Z + n jets and $t\bar{t}$ + n jets, with $n \leq 6$ as well as single top + jets backgrounds.

We showed a summary table of the search performance for various choices of stop and neutralino masses. We find that at $\sqrt{s} = 8$ TeV, in such a scenario, it is possible to reduce background down to a level of signal cross section for stop masses around 350-500 GeV for a $\tilde{\chi}_1^0$ mass of 100 GeV.

In the Bino-Higgsino dark matter scenario, $\tilde{\chi}_1^0$ is a mixture of Bino and Higgsino, satisfying the thermal dark matter relic density. $\tilde{\chi}_{2,3}^0$ is considered to be mainly Higgsinos. All three are lighter than $\tilde{t}$, which is in the sub-TeV range. In such a scenario, an interesting decay chain of stop is $\tilde{t} \to t\tilde{\chi}_{2,3}^0$, followed by $\tilde{\chi}_2^0 \to l^\pm \tilde{l}^{(*)\mp} \to l^\pm l^\mp \tilde{\chi}_1^0$ (via an intermediate slepton in "light slepton" case) or $\tilde{\chi}_2^0 \to Z\tilde{\chi}_1^0 \to l^\pm l^\mp \tilde{\chi}_1^0$ (via (off-shell) Z boson in "heavy slepton" case). The final states in $\tilde{t}\tilde{t}^*$ events have at least 2 jets, 2 opposite-sign same flavor leptons and missing energy. We also require at least one b-tagged jet to inferring the production of a third-generation squark.

Significances at LHC8 for discovering such a scenario are calculated in both light slepton case and heavy slepton case. In the light slepton case, The opposite-sign same flavor dilepton mass distribution after subtracting the opposite-sign different flavor distribution shows a clear edge. A discovery sensitivity up to 600 GeV of $m_{\tilde{t}}$ with 30 fb^{-1} of integrated luminosity at the LHC8 is expected. If the Higgsino component in $\tilde{\chi}_1^0$ is reduced, then one needs coannihilation processes to satisfy the relic density. In such a case, the p_T of leptons becomes lower and the significance of the study is decreased. In heavy slepton case, dileptons are produced from the (off-shell) Z boson decay. Small branching fraction of $\mathcal{B}(Z \to ll)$ results in decreasing the discovery sensitivity, compared to the light slepton case.

Although we did not show the expected experiment mass reach at 14-TeV, a similar study can be performed at LHC14. It is planned that the LHC will deliver an integrated luminosity of up to 3000 fb^{-1}, which requires upgraded ATLAS and CMS detectors, but the exact detector configurations are not finalized. Therefore, given that the background estimation and signal extraction strategies would be largely dependent on the upgraded detector designs and trigger conditions, systematic uncertainties driven by the high pile-up conditions have not been considered as they are highly dependent on the ability to reject pile-up jets. This is beyond the scope of this dissertation.

In the compressed scenario ($\Delta m = m_{\tilde{t}} - m_{\tilde{\chi}_1^0} \sim m_t$), traditional search strategies that rely on $\not{E}_T$ to reduce $t\bar{t}$ background have poor performance. We provide a feasible strategy using VBF topology selection in such a scenario. The $\tilde{\chi}_1^0$ in our studies is mostly Bino, while the $\tilde{t}$ is mostly $\tilde{t}_R$ such that the dominant decay mode of the $\tilde{t}$ is either $\tilde{t} \to t\tilde{\chi}_1^0$ ("two-body decay" case, when mass difference is slightly greater than the top quark mass), or $\tilde{t} \to bW\tilde{\chi}_1^0$ ("three-body decay" case, when the mass difference is smaller than the top quark mass).

We perform the study for both two-body decay and three-body decay cases in the final state of two b-jets, one lepton, large missing energy, and two high energetic VBF tagging jets with large separation in pseudo-rapidity, in opposite hemispheres, and with large dijet mass. A major improvement over non-VBF searches is the efficiency of the $\not{E}_T$ cut, due to the fact that top squarks are produced with a pair of high p_T tagging jets, and the momentum of the particles centrally produced in the $\tilde{t}$ system, importantly the $\tilde{\chi}_1^0$, have to balance the p_T of the incoming partons. Our study shows that the broad enhancement of $\not{E}_T$ and the requirement of two VBF tagging jets are very effective in reducing SM backgrounds.

Significances are evaluated at luminosity 300, 1000, and 3000 fb^{-1} of 14-TeV LHC for different top squark masses in both two-body decay case and three-body decay case. In two-body decay case, our studies show that there is discovery reach up to 340 (390) GeV for an integrated luminosity of 1000 (3000) fb^{-1} at 14 TeV. In three-body decay case, For $\Delta m \sim 165$ GeV, the discovery potential is up to 310 GeV for an integrated luminosity of 1000 fb^{-1} at 14 TeV. Both discovery reaches are outside the optimistic discovery projections of CMS and ATLAS searches.

In three-body decay case, we have assumed efficient identification of b-jets down to $p_T \sim 20$ GeV.

However, we note the ability to identify low p_T b-jets requires further study under the harsh pileup conditions of the 14 TeV LHC which is beyond the scope of this dissertation. We merely stress good tagging efficiency down to $p_T \sim 20$ GeV as a crucial requirement in the three body decay near the compressed regions, when the b-jets become soft.

Although some benchmark points in our studies may have already been excluded by LHC8, our search strategies work for bigger $\tilde{t}$ masses. If $\tilde{t}$ is heavier, higher experiment luminosity will be required.

REFERENCES

[1] CMS Collaboration, S. Chatrchyan *et al.*, JHEP **1306**, 081 (2013), hep-ex/1303.4571.

[2] ATLAS Collaboration, G. Aad *et al.*, Phys.Rev. **D87**, 012008 (2013), hep-ex/1208.0949.

[3] ATLAS Collaboration, G. Aad *et al.*, JHEP **1207**, 167 (2012), hep-ex/1206.1760.

[4] CMS Collaboration, S. Chatrchyan *et al.*, Phys.Rev.Lett. **109**, 171803 (2012), hep-ex/1207.1898.

[5] ATLAS Collaboration, ATLAS-CONF-2013-047.

[6] ATLAS Collaboration, ATLAS-CONF-2012-166.

[7] ATLAS Collaboration, ATLAS-CONF-2012-167.

[8] ATLAS Collaboration, ATL-PHYS-PUB-2013-007, ATL-PHYS-PUB-2013-011.

[9] CMS Collaboration, (2013), hep-ex/1307.7135, CMS-NOTE-13-002.

[10] B. Dutta, T. Kamon, A. Krislock, K. Sinha, and K. Wang, Phys.Rev. **D85**, 115007 (2012), hep-ph/1112.3966.

[11] B. Dutta, T. Kamon, N. Kolev, K. Sinha, and K. Wang, Phys.Rev. **D86**, 075004 (2012), hep-ph/1207.1873.

[12] B. Dutta *et al.*, Phys.Rev. **D87**, 095007 (2013), hep-ph/1302.3231.

[13] B. Dutta *et al.*, (2013), hep-ph/1312.1348.

[14] P. Gondolo *et al.*, (2002), astro-ph/0211238.

[15] F. E. Paige, S. D. Protopopescu, H. Baer, and X. Tata, (2003), hep-ph/0312045.

[16] T. Sjostrand, S. Mrenna, and P. Z. Skands, JHEP **05**, 026 (2006), hep-ph/0603175.

[17] J. Conway, (http://www.physics.ucdavis.edu/~conway/research/software/pgs/pgs4-general.htm). PGS4 is a parameterized detector simulator. we use version 4 in the LHC detector configuration.

[18] B. Dutta, T. Kamon, N. Kolev, and A. Krislock, Phys.Lett. **B703**, 475 (2011), hep-ph/1104.2508.

[19] B. Dutta, T. Kamon, A. Krislock, N. Kolev, and Y. Oh, Phys.Rev. **D82**, 115009 (2010), hep-ph/1008.3380.

[20] CMS Collaboration, S. Chatrchyan *et al.*, Eur.Phys.J. **C71**, 1721 (2011), hep-ex/1106.0902.

[21] CDF Collaboration, Do Collaboration, Z. Ye, (2011), hep-ex/1107.4539.

[22] M. L. Mangano, M. Moretti, F. Piccinini, R. Pittau, and A. D. Polosa, JHEP **0307**, 001 (2003),

hep-ph/0206293.

[23] N. Arkani-Hamed, A. Delgado, and G. Giudice, Nucl.Phys. **B741**, 108 (2006), hep-ph/0601041.

[24] C. Cheung, L. J. Hall, D. Pinner, and J. T. Ruderman, JHEP **1305**, 100 (2013), hep-ph/1211.4873.

[25] P. Grothaus, M. Lindner, and Y. Takanishi, JHEP **1307**, 094 (2013), hep-ph/1207.4434.

[26] M. Perelstein and B. Shakya, Phys.Rev. **D88**, 075003 (2013), hep-ph/1208.0833.

[27] M. Farina *et al.*, Nucl.Phys. **B853**, 607 (2011), hep-ph/1104.3572.

[28] R. Allahverdi, B. Dutta, and K. Sinha, Phys.Rev. **D86**, 095016 (2012), hep-ph/1208.0115.

[29] I. Gogoladze, F. Nasir, and Q. Shafi, Int.J.Mod.Phys. **A28**, 1350046 (2013), hep-ph/1212.2593.

[30] J. Alwall, M. Herquet, F. Maltoni, O. Mattelaer, and T. Stelzer, JHEP **06**, 128 (2011), hep-ph/1106.0522.

[31] CMS Collaboration, S. Chatrchyan *et al.*, Phys.Lett. **B718**, 815 (2013), hep-ex/1206.3949.

[32] CMS Collaboration, (2013), CMS-PAS-BTV-13-001.

[33] CMS Collaboration, A. Dominguez *et al.*, (2012), CERN-LHCC-2012-016, CMS-TDR-11.